ELECTRICAL CHARACTERIZATION OF SPHERICAL COPPER OXIDE MEMRISTIVE ARRAY SENSORS

THESIS

James P. Orta, Second Lieutenant, USAF

AFIT-ENP-14-M-40

DEPARTMENT OF THE AIR FORCE
AIR UNIVERSITY

AIR FORCE INSTITUTE OF TECHNOLOGY

Wright-Patterson Air Force Base, Ohio

AFIT-ENP-14-M-40

ELECTRICAL CHARACTERIZATION OF SPHERICAL COPPER OXIDE MEMRISTIVE ARRAY SENSORS

THESIS

Presented to the Faculty

Department of Electrical and Computer Engineering

Graduate School of Engineering and Management

Air Force Institute of Technology

Air University

Air Education and Training Command

in Partial Fulfillment of the Requirements for the

Degree of Master of Science in Electrical Engineering

James P. Orta, B.S.E.E.

Second Lieutenant, USAF

March 2014

AFIT-ENP-14-M-40

ELECTRICAL CHARACTERIZATION OF SPHERICAL COPPER OXIDE MEMRISTIVE ARRAY SENSORS

James P. Orta, B.S.E.E.
Second Lieutenant, USAF

Approved:

//signed//	13 March 2014
Major Timothy W.C. Zens, PhD (Chairman)	Date
//signed//	13 March 2014
Alex G. Li, PhD (Member)	Date
//signed//	13 March 2014
Ronald A. Coutu Jr., PhD, PE (Member)	Date

Abstract

A new System Protection (SP) technology is explored by using electrical and mechanical interference-sensing devices that are implemented with granular memristive material. The granular materials consist of oxide-coated copper spheres with radii of about 700 μm that are placed in contact to produce thin oxide junctions which exhibit memristive behavior. Processes for etching, which compared acetic acid and nitric acid etches, and thermal oxidation at 100 °C are performed and compared to produce copper spheres with a copper oxide layer over the sphere surface. Oxidized copper spheres are tested as sensor arrays by loading into a capillary tube in an aligned arrangement. The spheres are held in contact to characterize current-voltage behavior for various oxide thicknesses with typical R_{OFF} values in the MΩ range. It is shown that increasing the number of spheres in a chain causes a linear increase in breakdown voltage. Electrical characterization of the oxidized copper spheres reveal directly proportional changes to current-voltage hyseteresis in μW under compressive forces up to 22.3 mN. The thinnest oxide exhibited changes of 8.3 to 21.2 μW over 9 mN of compressive force while the thickest had a response from 0.4 to 2.5 μW over 22.3 mN of compressive force.

The effort and focus put into this work is dedicated to those who supported me in the long process of scuplting this research into a complete document. I specifically want to thank my best friend, Alessandra.

Acknowledgments

This culmination of effort was possible because of the great many people who held an interest in my development as an engineer and as an officer. I could not have done this work without them. I thank Mr. Greg Smith and Mr. Mike Ranft for sharing their expert knowledge and their willingness to help. I thank Dr. Kent Averett for teaching and assisting with the X-ray diffractometry. I thank Dr. Sarah Francis for teaching and assisting with the operation of the electrical measurement equipment. I thank Dr. Daniel Felker for providing assistance with the scanning electron microscopy. I thank Dr. Coutu for sharing his wisdom and helping me hone my intuitive thinking and problem solving skills. I thank Dr. Li for his guidance and encouraging my creativity by engaging in several conversations on the possibilities of this research. Finally, I thank Major Zens for his mentorship, advice, and unrelenting positive attitude.

James P. Orta

Table of Contents

Page

Page

List of Figures

List of Tables

List of Symbols

Symbol	Definition
d	thickness (meters)
I	current (amps)
M	memristance (ohms)
Q	charge (coulombs)
R	resistance (ohms)
R_a	arithmetic average roughness (nm)
R_q	RMS roughness (nm)
R_{max}	maximum roughness (nm)
T	temperature (kelvins, degrees celsius)
t	time (seconds)
V	voltage (volts)
Φ	flux linkage (Weber)
Z_{range}	Height range (nm)

List of Chemical Symbols

Symbol	Definition
Al	aluminum
Ar	argon
C	carbon
CH_3COOH	acetic acid
Cu	copper
$Cu(CH_3COO)_2$	cupric acetate
CuO	cupric oxide
Cu_2O	cuprous oxide
H_2	hydrogen gas
H_2O	water
HNO_3	nitric acid
N_2	nitrogen gas
NO_2	nitric oxide
NO_3	nitrous oxide
O_2	oxygen gas
Pt	platinum
Ti	titanium
TiO_2	titanium oxide
W	tungsten

List of Acronyms

Acronym	Definition
AFM	Atomic Force Microscopy
APS	Active Protection System
BSE	Back-Scattered Electron
CCD	Coded Control Device
CDS	Command Disablement System
DoD	Department of Defense
ESM	Electrochemical Strain Micrscopy
PAL	Permission Action Link
SE	Secondary Electron
SEM	Scanning Electron Microscope
SP	System Protection
TEM	Transmission Electron Microscopy
WMD	Weapons of Mass Destruction
XRD	X-Ray Diffractometer

ELECTRICAL CHARACTERIZATION OF SPHERICAL COPPER OXIDE MEMRISTIVE ARRAY SENSORS

I. Introduction

1.1 Background: Sensitivity of Defense Technologies and WMDs

Among the most important aspects of defense strategy is the safe and secure storage and transport of Weapons of Mass Destruction (WMD). The purpose of using stringent security measures for WMDs and WMD-related material is to prevent unauthorized access and abuse [13]. The big push for secure storage originated when President Kennedy issued a memo that ordered complete control of America's entire nuclear arsenal using technical means [1]. As nonproliferation treaties began, so did the establishment of systems to ensure and monitor compliance. Treaties and regulatory agencies provided guidelines for protecting nuclear materials [13, 41]. This improvement in control has been the drive of an entire sector of security engineering technologies for the past 60 years [1].

Measures taken by the Department of Defense (DoD) to protect U.S. weapons systems need to adapt as the technology used for system intrusion advances in order to protect weapons systems from exploitation by the enemy. As directed by DoD 5200.1-M, the use of effective countermeasures for the security of critical technologies is mandatory [9]. However, Huber and Scott point out that former interpretations of this directive fails to achieve program protection for the entirety of the weapon system's lifetime, including the weapon system's deployment phase and retirement [12]. There is a need to research technologies that have the potential to protect weapon systems from intrusion and exploitation.

Some System Protection (SP) technologies that are currently in use are encryption methods, protective materials, hardware access denial systems, and self-destruct mechanisms that safely disable detonation components [12]. Specifically, current technology implements a task referred to as "use control," which involves security measures that prevent unauthorized use [30]. Among the design features for control use are a Coded Control Device (CCD), Command Disablement System (CDS), Active Protection System (APS), an environmental sensing device, and a Permission Action Link (PAL). Altogether, these component systems provide a high-technology implementation of the Authorization-Environment-Intent rule mentioned by Anderson [1]. Among these component systems, the only system that detects physical attempts to gain unauthorized access is the APS. The APS prevents any unauthorized access by sensing interferences and causing physical damage to critical components [30]. The function of interest in this technology is the manner in which critical components are damaged and disabled; however, technical details for this system are classified [33].

SP technologies require continuous innovation in order to maintain vigilance against an adaptive adversary. When possible, it is sensible to reassess current technologies for their potential for improvement or replacement in current SP systems. As mandated by several treaties and agreements, protecting nuclear materials is a matter of nonproliferation and requires the effective use of SP technologies in order to protect against theft and exploitation [13]. The threat of any unauthorized access to WMDs drives the need for integrated technologies that can detect system interferences on multiple levels to account for physical and electronic intrusion. Implementing effective, state-of-the-art SP technologies is a necessary and critical component in threat reduction and requires continual research.

1.2 Problem Statement: Spherical Memristors for Sensing Interferences

An SP technology for protecting WMDs should be adaptable and resilient. Such an SP technology would require a multi-level approach to sensing interferences that may indicate an attempted exploitation, break-in, or other effects that may compromise security. In the event of any of these interferences, an SP system would need to detect physical or electronic changes of several types.

The SP technology being investigated uses a memristive system to serve as a sensing network for detecting electrical or mechanical interferences. This system consists of copper spheres with a cuprous oxide covering the surfaces. By close-packing groups of these metal spheres, chains of $Cu/Cu_2O/Cu$ contact points are created between the oxide layers. These contacts serve as the basis of the memristive elements. Figure 1.1 provides a visual of what each contact will provide.

A secondary sphere made of an insulating material will also be used in the close-packing system. These insulating spheres will cause force chains and electrical connections to occur in more direct routes. These direct routes and force chains will be the medium in which an applied signal can read the electronic state of the system and determine whether interference has occurred. The memristive copper spheres are expected to operate in a 3-dimensional close-packing system of binary spheres in which one sphere type operates like a semiconductor and the other is insulating. The random arrangement of the spheres would result in a specific electrical signal. In a starting position, an electrical signal can be briefly applied to the system and an output signal can be periodically checked to ensure the arrangement of the spheres has not been altered. If the spheres experience interference, the output signal will change. In the event of a mechanical interference, the positions of the spheres will shift in such a way that the electrical contacts (including contact areas) between spheres change, resulting in a different signal output.

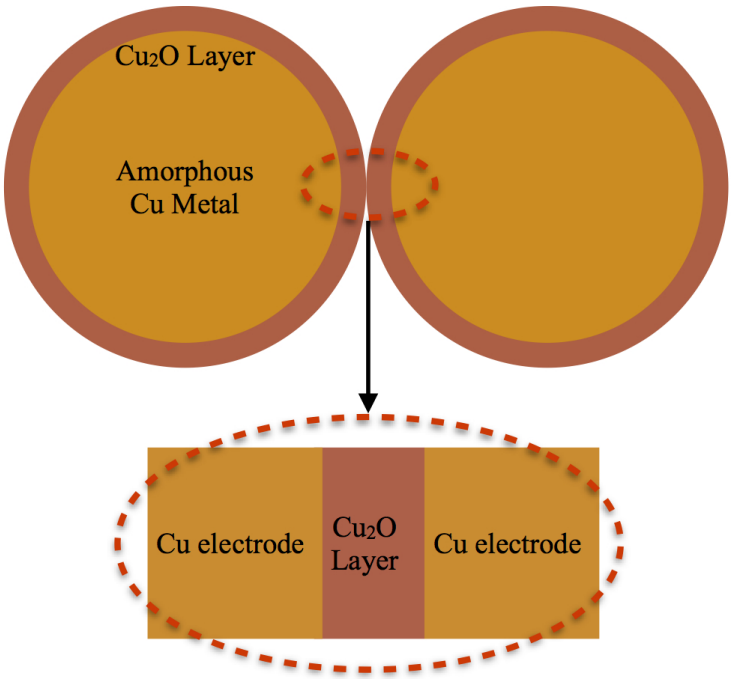

Figure 1.1: Contact junction of cuprous oxide spheres. The copper spheres develop a natural oxide on the surface. Two spheres can form a contact junction. The junction creates a metal/oxide/metal interface that function as a memristive device. Adapted from [22].

An electrical interference would result in a change in the electrical signal by changing the electrical history of the memristive network. These events are demonstrated in Figure 1.2.

The reliable operation of this memristive network will require a strong understanding of the electrical characteristics of the spherical cuprous oxide memristors. The general behavior of memristors has been intensively studied since their physical realization in 2006 [38]. While much has been learned about memristors, they have all been explored on a flat substrate with generally rectangular dimensions. The memristive interfaces in this research will be at the surface of copper spheres, which is a novel implementation of the memristor since traditional memristive devices are built on a planar substrate. It will be necessary to gather data that describes the electrical behavior of the spheres. It will be important to understand how the current flows through the spheres when a voltage is

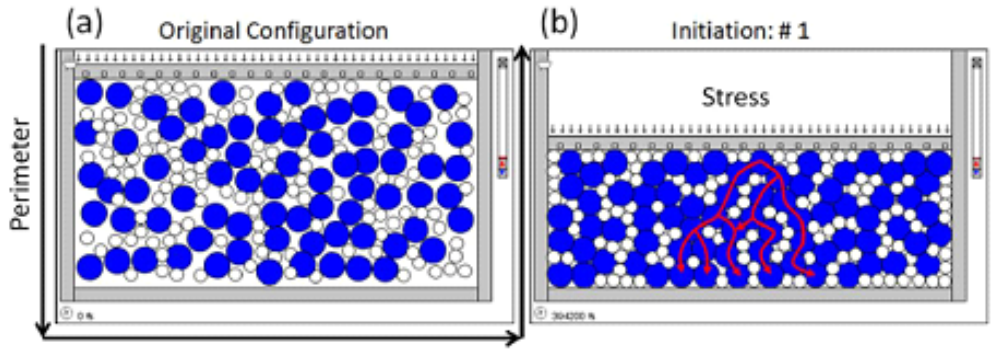

Figure 1.2: A simple simulation of compacting a system of binary spheres in an original configuration and then under a compressive stress. The spheres can be initiated into a unique position. In the event of a mechanical interference, the positions of the spheres will shift in such a way that the electrical contact between spheres change, resulting in a different signal output. Each initiation results in a new unique configuration [22].

applied, the capacitive properties of the oxide layer and how they will affect the electrical behavior, and how these electrical behaviors will change when a mechanical stress is applied to the system.

To achieve reliable results when characterizing the electrical properties of the memristive system, the copper spheres must be processed. The copper spheres were distributed by Industrial Tectonics Inc. and manufactured by Canfield Technologies using a proprietary fabrication method. As received, the copper spheres may have contaminants throughout the oxide surface and composition that will require cleaning. A clean surface is preferable for hosting the growth of oxide layers for each sphere. In order to accurately characterize the electrical properties, it will be necessary to create a process that can grow oxide layers in a consistent manner. With a standardized cuprous oxide sphere, it will be possible to apply the findings of the electrical characterization to all cuprous oxide spheres that went through the same process.

1.3 Scope: A 1-Dimensional Array of Spherical Cuprous Oxide Memristors

This project uses a 3-dimensional close-packing system of binary spheres; however, in order to characterize the memristive spheres, it will be necessary to characterize the device in a simpler context. Several complexities can arise by arranging these spheres in 2- or 3-dimensional arrays, which may complicate the process of characterizing them. For this reason, research will be done to characterize the spheres in a 1-dimensional array of spheres. In such a set up, a row of memristive spheres would essentially be parallel memristor-capacitor pairs in series with resistors. Figure 1.3 shows an equivalent circuit of a system consisting of two spheres.

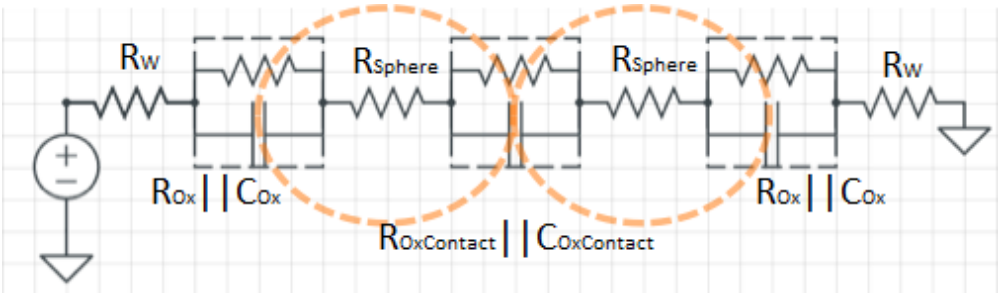

Figure 1.3: Two spheres in series. Current will conduct in a similar way that this superimposed equivalent circuit would. In this diagram, the parallel resistor and capacitor represent the oxide layer interfaces which will behave with memristive characteristics.

The scope of this project assumes that the behaviors and characteristics of simple sphere chains will inform more complex arrays of the spheres. Specifically, it is assumed that analyzing the 1-dimensional model will inform the 2- and 3-dimensional systems. This assumption is logical and necessary because reliably characterizing the spheres could not be achieved in a circuit of parallel spheres, which may dilute the output signal with circuit phenomena such as phase delay and signal attenuation.

This research will be used to provide groundwork for developing an SP system using spherical memristive devices. Research of the electrical characteristics of the

1-dimensional array will provide a working knowledge for researching 2-dimensional arrays and introducing a binary sphere system in which the other type of sphere will be insulating rather than conducting. The one-dimensional array will be tested to show that spherical cuprous oxide memristors can be used to sense mechanical and electrical interferences.

1.4 Overview of Thesis

This thesis will continue in Chapter 2 by providing a full description of memristors, including their materials, fabrication, and theory of operation. Chapter 2 will then continue to explain the electrical properties of cuprous oxide. Chapter 3 will explain the analysis, oxide surface processing, experimental set up, and the data that will be collected. Chapter 4 will discuss the results that were found during the characterization experiments. Chapter 5 will use the results to formulate a conclusion about the characterization of spherical cuprous oxide memristors in a 1-dimensional array, therein providing the necessary information to pursue device characterization in more complicated implementations.

II. Literature Review

2.1 Chapter Overview

The purpose of this chapter is to explain the history and fundamentals of the memristor. Particular topics that are pertinent to understanding a memristive device are the operation and the materials and processes that are used to fabricate them. The operation of a memristor involves two aspects of discussion: the theory of how ideal memristors work, and the actual behavior that has been documented by researchers. Similar to many other technologies, there are practical limitations to theoretical performance. There are a few disparities between the theory and the science. Although these differences may have small affects in most cases, it is still worth noting that the physical behavior of memristors varies slightly from theory. The materials and processes that are used to build memristors vary. Research has been done on using metal oxides, polymers, and magnetic materials [27]. The focus of this chapter will be the research of metal oxide-based memristors because they are most applicable to the copper oxide systems research.

2.2 Memristive Devices

Memristors have been a topic of scientific research since 1971 [6]. In the midst of Chua's work on founding the mathematical principles of nonlinear circuit theory, he had noticed that it would be possible to define a fourth passive two-terminal circuit element. With the first three the resistor, capacitor, and inductor being well defined in linear circuit theory, the fourth is defined with a nonlinear relationship. With four fundamental electrical phenomena to define as variables: voltage, current, charge, and flux, there are potentially six relationships that could be defined between any pair of variables. However, in linear circuit theory, there are only 5 equations that relate these to one another. Chua noted that one relationship that is not yet defined is that between charge and flux.

Figure 2.1 is a visual representation of the basic electrical relationships, showing all six relationships of circuit theory.

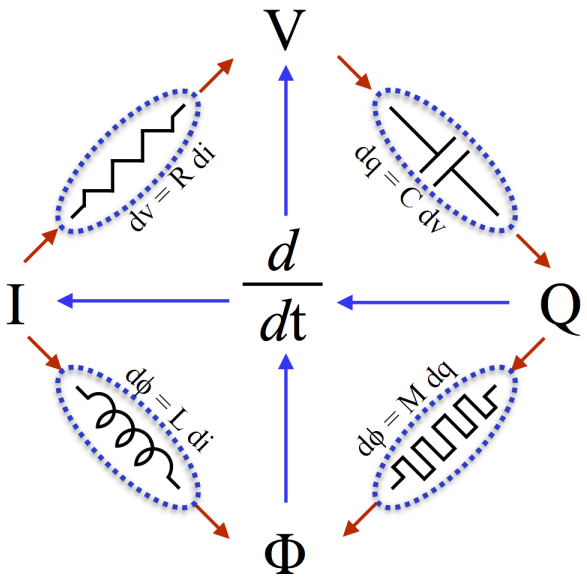

Figure 2.1: The electrical relationships between the fundamental circuit elements. Adapted from [38].

By generalizing these relationship to be nonlinear systems, Chua was able to indicate that whatever fundamental circuit element could relate charge and flux would do so by being a nonlinear variable resistor [6]. Such a passive variable resistor would be capable of memory effects [7]. As a proposal to fill the gap and for the sake of completeness in circuit theory, Chua suggested the memristor as a fundamental circuit element that relates charge and flux [6]. Chua showed that when relating charge and flux, what actually occurs is a nonlinear relationship between voltage and current such that

$$V(t) = M(q(t))I(t) \tag{2.1}$$

in which M(q(t)) is memristance, a nonlinear function of charge, V(t) is a voltage, and I(t) is the corresponding current [7]. This gives some insight to the fact that

memristance can be described as a specific value of resistance at any particular point in time [6]. However, if the relationship between charge and flux is linear, then the function of memristance simply becomes a constant, otherwise known as the resistance. Chua went further by strongly defining what makes a memristor. He concluded with 5 theorems, shown in Table 2.1 that define the rules that a device must follow in order to qualify as a memristor.

Table 2.1: The theorems of what a device must have in order to be a memristor [6]

Theorem	Explanation
Passivity Critereon	Is a passive device only if its incremental memristance is nonnegative
Closure Theorem	A network of memristors can be modeled as one memristor
Existence and Uniqueness	Any network of memristors has only one solution
Principle of Stationary Action	A vector of charge is a solution only if it represents a stationary point in time
Order of Complexity	The complexity of a memristive circuit is described by the number of elements, nodes, and connections

Although he had constructed the idea of a memristor, Chua had no prediction of a physical device that would create such an effect. While there had been several instances of what are now recognized as memristive characteristics, in 2006 Stan Williams team at HP

labs had identified electrical behaviors that they soon realized fit with Chua's theoretical memristor [46].

The discovery of memristive properties led HP Labs to begin investigating the memristor and perfecting the connection between what Leon Chua had theorized and the actual electrical phenomena. In their paper, "The missing memristor found," Strukov discusses how memristive effects occur in nature at the nano-scale [38]. In fact, while researching nano-scale devices that showed pinched hysteresis I-V curves, the HP Labs team began reading Chuas papers in hopes of trying to explain the cause for the unique current-voltage characteristic. They found that the pinched hysteresis curves could be explained by Chua's theoretical memristor. Chua followed up on his theory in 2010 to specify that a memristor can be identified by such hysteresis loops in the I-V curves and provided a simple mathematical tutorial of how these devices may work [7]. Figure 2.2 shows a hysteresis curve using equations similar to those discussed by Chua.

By defining flux as a monotonically increasing function of charge, and providing a sinusoidal voltage source, one can solve for a time-dependent function of current that, when plotted parametrically with voltage, creates a hysteresis plot. Their official discovery of the memristor took place when they found what caused the pinched hysteresis loop, and subsequently, the reason why the resistance changes [37]. As it turns out, the equation that was suggested by Chua was comparable to an expression that can describe the drift velocity of oxygen vacancies. This indicated that the physical construction of a memristor actually changes under bias and this additional ion flow is what causes the nonlinear change in resistance.

2.3 Theory of Memristors

The memristor was theorized almost completely on a mathematical basis until 2006. The theorems mentioned in Table 2.1 provide a strong insight to the rigorous definition

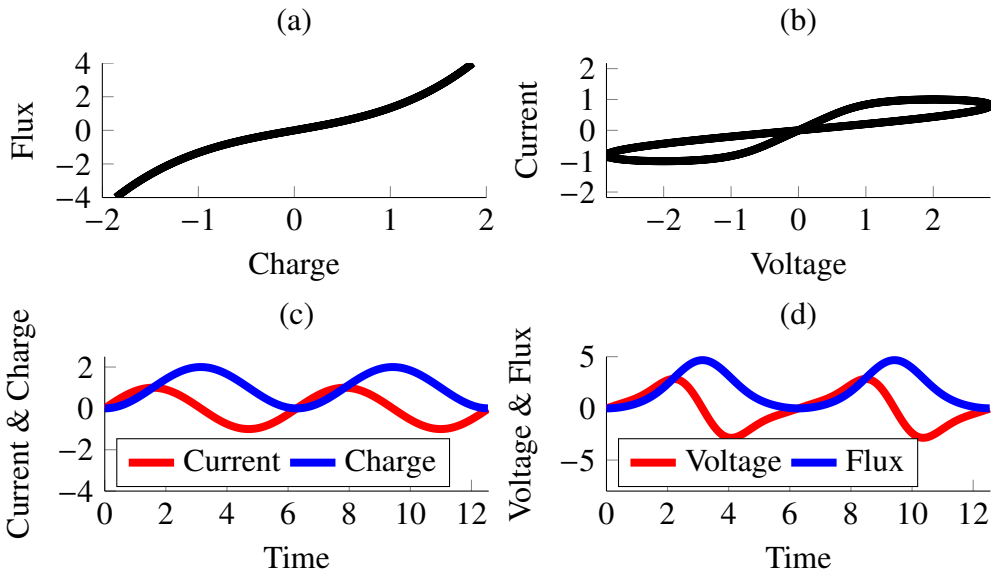

Figure 2.2: The hysteresis loop is characteristic of memristive devices. In 2010, Chua provided a mathematical tutorial on the hysteresis loop in the I-V curve for memristors. This particular plot is defined by (a) the flux-charge relationship of $\phi = q + q^3/3$. In (c) and (d) the current and voltage signals are shown with their antiderivatives charge and flux, respectively. The current has a signal $I = \sin t$ and results in (b) the I-V curve. Adapted from [7].

that was given to memristors. However, these theorems did not provide a physical insight of the electrical workings of device function. As indicated in the previous section, the cause for the hysteresis curve was a mystery until the HP Labs team discovered that a voltage not only caused electrons and holes to move through the device, but it caused ions and oxygen vacancies to move as well. This ionic transport physically changes the device composition, which in turn, adjusts the resistance [46]. Figure 2.3 shows a diagram of a simplified memristor operation as discovered by HP Labs.

This discovery served as a stepping-stone for the research and development of a refined and engineered memristor design. Much of the memristor research performed by HP Labs has been done using Titanium dioxide, which is a transition metal-oxide with a band gap of about 3 eV. Through their research efforts, HP Labs and their partners have

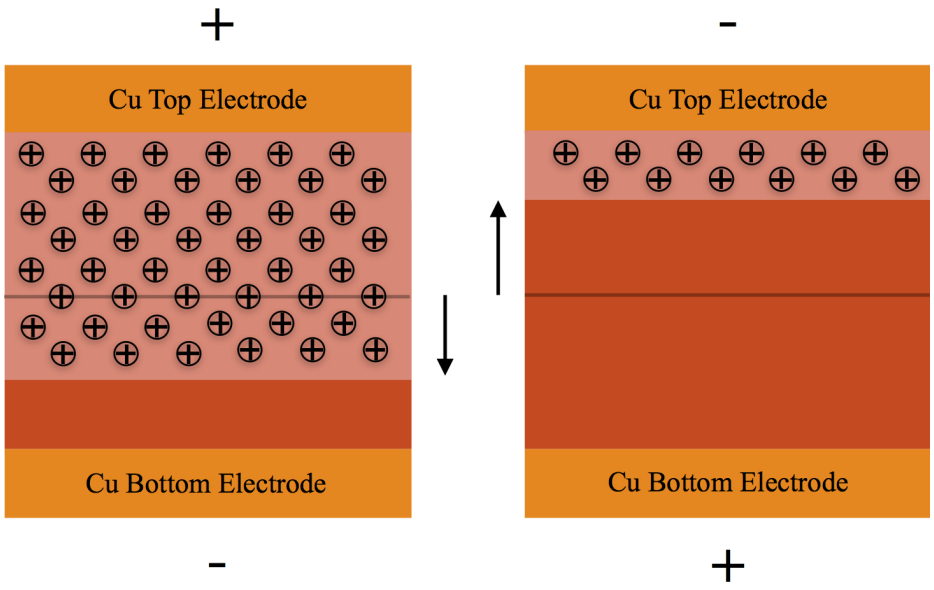

Figure 2.3: This image depicts the movement of ion and ion vacancies when a positive or negative voltage is applied. The movement of the positively charged ions or ion vacancies causes a change in resistance that occurs continuously. As a positive voltage is applied to one side, the ions or ion vacancies are pushed throughout the length of the memristor, causing a decrease in resistance. Applying a negative voltage pulls the ions and ion vacancies back to the cathode side which then increases the resistance. Adapted from [46].

developed the beginnings of a theory of how memristors operate on a physical level that agrees with Chua's theory [52]. As Figure 2.4 shows, a memristor can be visualized as a pair of resistors in series in which the total series resistance can be controlled by a single slider in the middle, which can switch continuously between R_{ON} and R_{OFF} [38]. Assume in this example that having the arrow pointing in the middle of the resistors R_{ON} and R_{OFF} indicates that the current only passes through half of each resistor's value of resistance. When the slider is moved slightly to the right such that the arrows are pointing one-fourth from the right side of each resistor, then the current sees a resistance of 3/4 of R_{ON} and 1/4 of R_{OFF} and the total resistance is the series sum of those two values. Finally, if the slider is moved all the way to the right, the current passes through just R_{ON}, and thus total

resistance of the memristor is R_{ON}. The effects are similar for the slider analogy when moved left and approaching the other extreme value, R_{OFF}.

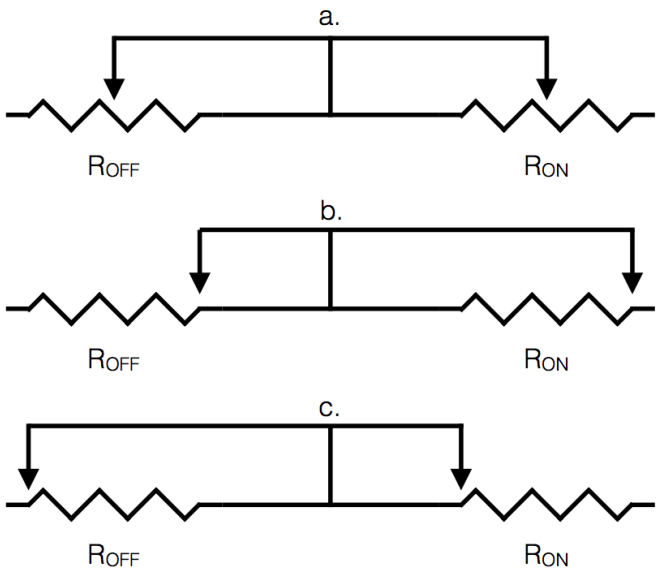

Figure 2.4: A simplified depiction of memristor operation. As a series circuit with a memristor has a voltage applied, the oxygen vacancies in the undoped cathode mobilize, causing a change in resistance. This can be compared the set of variable resistors that are shown. As a voltage is applied, the slide moves either up or down, providing a continuum of resistances between the values of R_{ON} and R_{OFF}. Adapted from [38].

Since the resistance R is the ratio of voltage and current, this means that the I-V curve's slope will be changing. This change results in a hysteresis plot very similar to that shown in Figure 2.2. In essence, a memristor is ideally a voltage-controlled, two-terminal variable resistor. A memristor will generally have an I-V curve with a pinched hysteresis loop. These characteristics are noticeable because of the very small scale (the nano-scale) that the devices are built on. Such memristive behavior would not be traceable in devices of considerably greater size (such as the millimeter-scale). Additionally, not all materials will have the same memristive behavior. The specific kinds of materials and fabrication techniques play a critical role in the development of proper devices.

2.4 Operation of Memristive Devices

The discovery of a potential memristive device prompted research on several topics in an effort to characterize the mechanisms of memristors. Several aspects of the device function have been established and researched but are not fully understood. Some aspects of device operation that are notably important are the dynamics of resistance switching, the electroforming process, and the effects on switching polarity and stability.

2.4.1 Electroforming

When first implementing a memristive device, HP Labs noticed a need to "wear in" the device before it was ready to operate [47]. In 2008, it was suggested that the forming of a conducting bridge as an important step in preparing a resistance switching device [11]. The formation of this conducting bridge or path, referred to as electroforming, is a process in which an applied electric field causes a soft dielectric breakdown to form a conductive path in the memristive material. These behaviors have been noted back to 1970 [8]. It has been shown by many that memristive devices require an electroforming process in order to operate [11, 54]. This electroforming process is necessary because many memristive materials naturally have an insulating effect, inhibiting current flow. The electroforming process creates vacancies where ions have been reduced along a channel within the bulk oxide. For this reason, it is largely suggested that the electroforming process is an electrochemical reduction of the material [11, 50]. Fujiwara showed that a conductive bridge could be formed by applying a voltage to an as-prepared planar metal/CuO/metal device in which the metal was either platinum or nickel [11]. Along with Transmission Electron Microscopy (TEM) images that show the conductive bridge, their research suggested that the conductive bridge was metallic. This was demonstrated by showing the relationship between device resistance and temperature, which behaved metallically in the low resistance state. Additionally, it was revealed that applying too

large of a bias resulted in dielectric breakdown, which puts the material in an irreverible resistance state. Figure 2.5 shows these states.

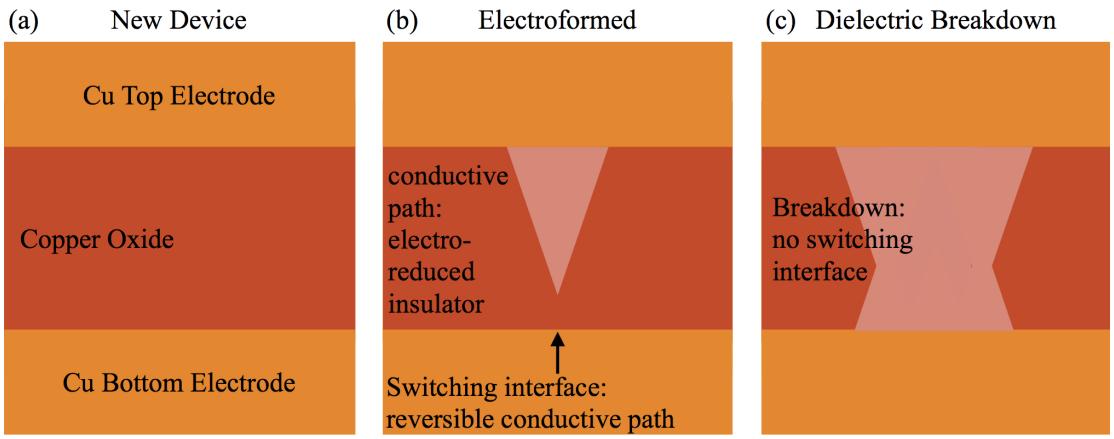

Figure 2.5: A simple depiction of (a) a new device and the changes that occur during electro-reduction processes. With enough energy, one can achieve (b) an electroformed device. However, with a considerable electric field strength, a device undergoes (c) dielectric breakdown. Adapted from [28].

Yang has shown that in TiO_2 devices, the electroforming process results in the creation of oxygen gas bubbles from the oxide and concluded that the process is an electro-reduction process that creates conductive channels of oxygen vacancies through the oxide [50]. Yang also detailed the events that occur while electroforming a TiO_2 memristor and suggested a method of engineering devices such that the electroforming process could be eliminated [50]. The electroforming process, by nature, involves a degree of randomness based on where and how the conductive channel is created [28]. As Yang comments, the electroforming process therefore causes a considerable about of variation between otherwise similar devices, harming experimental repeatability [50]. By demonstrating the electro-reduction that occurs during electroforming, it was possible to engineer the memristive devices to not require an electroforming step. It was shown that by designinging the devices to be thinner, which eliminates the bulk region and keeps the

switching interface, an electroforming process was no longer needed. Additionally, it was shown that by fabricating a device with a highly reduced oxide layer, such that the device is effectively built with conductive channel already in the bulk oxide, electroforming was not necessary to operate the device [50].

Today, HP Labs' memristor design uses titanium dioxide in two layers: an undoped layer (oxygen-deficient TiO_{2-x}), and a doped layer (oxygen-rich TiO_2) [38, 52]. These two layers achieve the conductive channel properties needed to not require such an electroforming step, thereby improving device repeatability and improving studies done on the resistance switching properties of memristors [47].

2.4.2 Resistance switching

The resistance switching mechanism is the primary behavior of a memristor [6, 7]. In Chuas theoretical model, the resistance switching occurs as a mechanism of flux- and charge-controlled actuation [6]. Interestingly, such resistive switching has been noted even before Chua theorized the memristor [8, 28]. The recent development of the memristor by HP Labs has been using TiO_2 in which the resistance switching occurs as a mechanism of ionic drift [38]. However, there are indeed multiple mechanisms that caused voltage- or current-controlled resistance switching [27]. Using metal-oxide memristive systems, however, these switching mechanisms act on a continuum of two main effects: electric fields and Joule-heating [36, 48].

2.4.2.1 Field-dominated Memristors

The discussion on memristors has so far focused on field-dominated devices. Field-dominated devices tend to exhibit a bipolar switching mechanism, meaning that the resistance switching occurs with a dependence on the voltage polarity [52]. This dependence stems from the dominating effects that electric potential and electron kinetic energy have on the resistance switching.

These effects may be stronger in some materials than others. Kim used I-V curves and Electrochemical Strain Micrscopy (ESM) to observe the onset of ionic motion in NiO devices [18]. In these devices, a voltage sweep from -10 to 10 V produced a noticeable, but relatively small hysteresis loop. Comparatively, Pickett's titanium oxide devices exhibit much larger hysteresis loops, ranging in several orders of magnitude in current [32]. These differences in behavior may be attributable to the different materials.

As mentioned previously, the mechanism of field-dominated resistance switching involves the contribution of an electric field and electron kinetic energy. Specifically, these phenomena result in ionic drift through the conductive channel (which was created by electroforming or in fabrication, as mentioned in Section 2.4.1). This ionic drift can consist largely from either ions or vacancies. Furthermore, the ions may derive from the semiconductor material or even from the electrode. Using Cu-SiO_2 cells, Schindler showed how copper ions from the electrode may have contributed to the formation and dissociation of the conductive channel [34]. Most commonly seen are conductive filaments consisting of the semiconductor material. By contrast, Pickett attributes the bipolar switching in TiO_2 devices to the drift and diffusion of the oxygen vacancies within the TiO_2 [32].

In general, the resistance switching mechanism works as polarity dependent electrochemical reduction process [35]. By applying a bias, ionic drift is initiated and switching occurs rapidly upon reaching a voltage, V_{SET} [44]. During this stage, an electric field is influencing the drift of ions or vacancies along the conduction channel toward either of the electrode interfaces [35]. Figure 2.6 shows the two primary states in which an electroformed device behaves. Upon reaching the SET position, the memristor reaches a low resistance state as the conductive channel reaches a length such that the remaining gap between the channel and the bottom electrode does not have a sufficient voltage drop to trigger further ionic drift [35]. The RESET operation occurs as a reverse-polarity bias is

applied to the device. The conductive channel undergoes a reversal of the SET process in which ions or vacancies drift back to their originating interface, effectively dissolving the conductive channel and returning to a high resistance state [44].

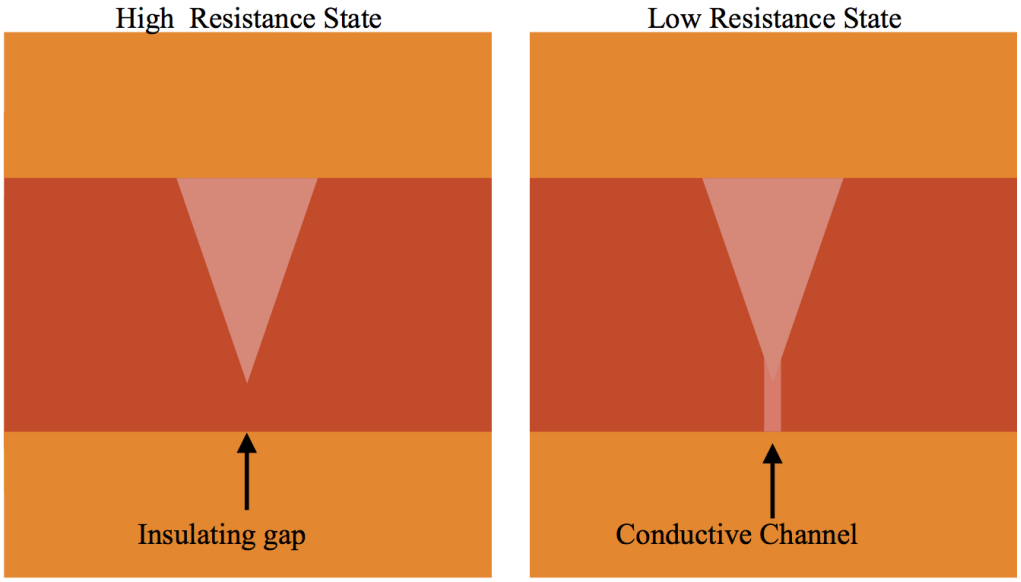

Figure 2.6: The low- and high-resistance states of a memristor. A device starting in a high resistance state switches to a low resistance state as an applied electric field induces an extension of a conductive channel where there was an insulating gap.

No memristor uses only electric-field induced switching [52]. There are, however, devices that operate purely by thermal-induced switching [36].

2.4.2.2 Thermal-dominated Memristors

The involvement of current almost certainly involves the potential for thermal effects caused by Joule-heating. It is a well known fact that metals exhibit a temperature dependent resistance. Joule-heating has been shown to play a large part in the conduction channel of oxide-based memristive devices as well [15, 35]. In fact, thermal-dominated memristors experience a resistance switching mechanism mainly as a result of Joule-heating. Kim made use of the role that thermal effects have to successfully model

the resistance switching mechanism in finite-element modeling [17, 35]. Since memristive devices are small, Joule-heating is in some way a factor for all resistance switching devices, and has even been shown to work in conducting polymers [49, 52]. Joule-heating occurs within memristive devices simply because the small area of the device results in a very large current density. Borghetti showed that temperature may act as one of many state variables involved in the resistance switching mechanism [2]. Indeed, it has been shown that electrically-induced heat gradients can cause device structures to deform, contributing to the resistance switching of the device [15]. This offers the possibility that thermal actuation may play a role in the conductive channel. Strachan reported the relationship of joule-heating with the location of the conductive channel where resistance switching occurs [35]. A diagram of how such resistance switching occurs is shown in Figure 2.7.

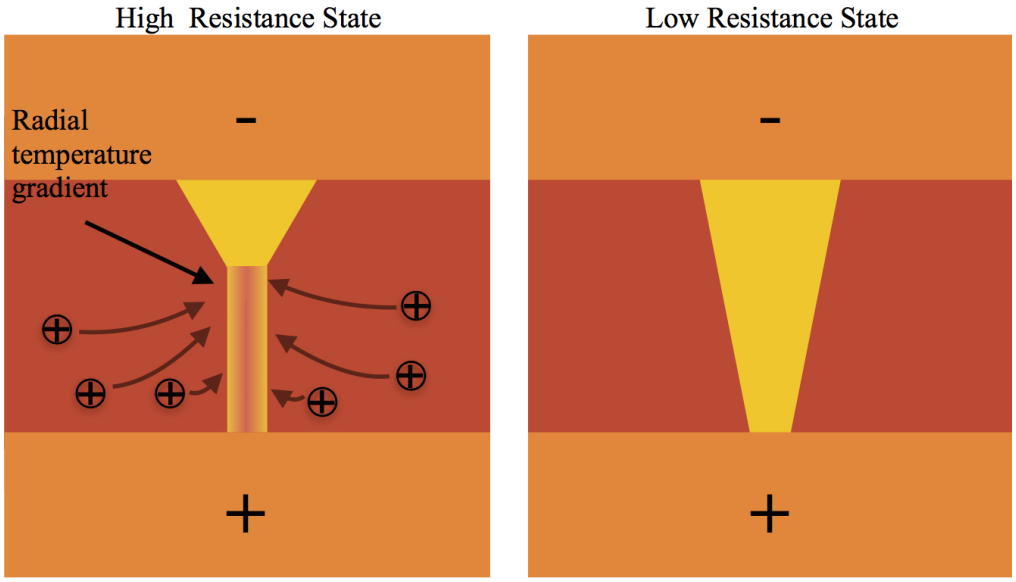

Figure 2.7: A depiction of ionic diffusion caused by a temperature gradient. High temperatures caused by Joule-heating enhances the drift and diffusion of electrons and may induce a mass transfer of atoms in a process known as thermophoresis. This ionic movement results in the formation of a conductive channel which allows for unipolar resistance switching. Adapted from [36].

The high temperatures caused by Joule-heating have been shown to enhance drift and diffusion and may induce a net mass transfer of atoms [36]. Even in field-dominated devices, a thermal gradient may speed up the motion of ionic drift and diffusion [15]. Strukov explains that thermophoresis, the diffusion of ions or vacancies in a temperature gradient, can be a result of such Joule-heating in the conductive channel [15, 36]. Specifically, it was shown that the SET operation of a memristor could be a result of thermophoresis [36]. This process would consist of a "formation and dissolution of a conducting channel" in which ions or vacancies diffuse to higher temperatures that would be occurring along the conductive channel. Ions or vacancies would then diffuse away from the conductive channel when the temperature gradient is small (even though the temperature may still be high).

Yang discusses the continuum of field-dominated memristors to thermal-dominated memristors and notes the gradual adjustment to a significant effort on the switching mechanism [52]. The increasing role with thermal effects leads to nonpolar switching in which reset switching is described as the thermal rupture of the conduction path [36]. In nonpolar switching (thermal-dominated), however, this thermal rupture repairs as the current is reduced, returning the device to a high-resistance state [52]. Alternatively, thermal-dominated devices may work with "threshold switching," a volatile switching mechanism with a hysteresis loop [36]. With this mechanism, Joule-heating from an increasing current causes a device to suddenly become ohmic, producing a jump in the I-V curve to very high current. The main attribute that dictates the memristive behavior is material [52]. Thus is it possible to design devices based on how they respond to thermal effects.

2.5 Materials and Fabrication

There are several materials and fabrication processes that can be used to build memristors. Before discovering Titanium Dioxide as their preferred material for building

a memristor, HP Labs was investigating molecular nonvolatile memory devices [46]. It seems that perhaps they were not too far off. Their research has led the way in motivating others to study the memristive effects in alternative materials. Some of these materials include polymers, ionic compounds, and other transition metal-oxide systems [27]. The most researched memristors are constructed with a transition-metal oxide, such as TiO_2. In this design of memristors, there is a single material with doped and undoped layers between ohmic contacts. Figure 2.8 shows a generic memristor with metal contacts and an insulating material. This fabrication diagram shows how a memristive device can implement two structures. One method uses a single layer of memristive material. The other method uses two layers of a doped-undoped interface that is sometimes used for devices not requiring an electroforming process.

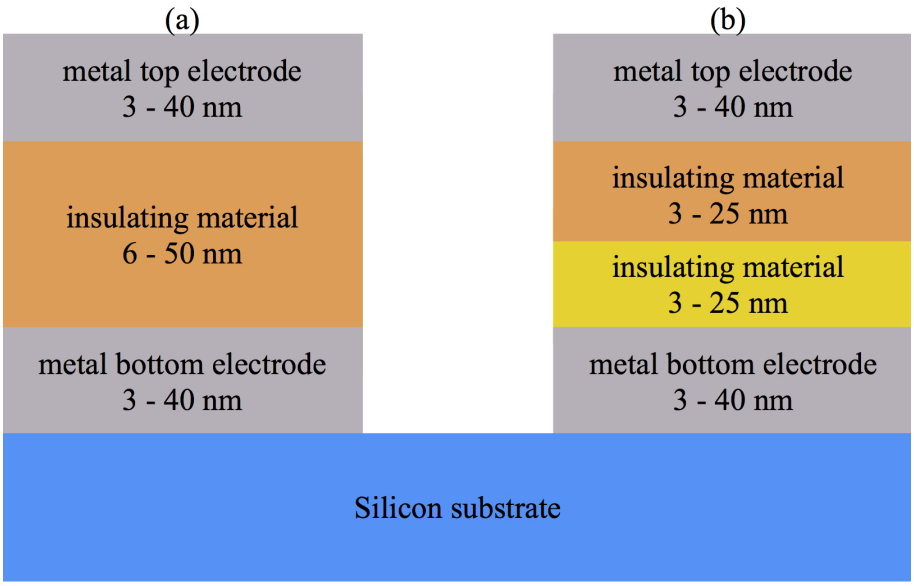

Figure 2.8: Fabrication diagram of generic memristor with metal contacts and insulating material.

For the metal-oxide implementation of memristors, the fabrication process is relatively simple. Early prototypes of intentionally built memristors utilized only the

simplistic approach described previously of layering single doped and undoped layers between two metal electrodes, such as that shown in Figure 2.8 [47]. However, after conducting tests on TiO_2 memristors, it was found that the specific path of ion migration was forming a conducting channel of Ti_4O_7, a stable compound of titanium and oxygen [54]. This discovery led to a new memristor construction that included a Ti_4O_7 filament placed within the length of the memristor. Figure 2.8 shows such a filament construction.

Like any other electrical device, there are specific processes involved in the device construction. Starting with a silicon substrate, electron-gun evaporation is used to deposit the electrode layer of either Titanium or Platinum [27]. Next, an undoped semiconductor layer is added, in this case a layer of TiO_2, by RF magnetron sputtering.

The same process is used to create the doped layer of Titanium dioxide except during the portion of the process oxygen is allowed to flow over the device. Finally, the top electrode is added using the same electron-gun evaporation process as the bottom electrode. Once the top electrode is added, the memristor is complete.

2.6 Copper Oxide Memristors

Copper oxide memristors are of particular interest to this research. Work has been done demonstrating the memristive behaviors of cupric oxide (CuO) and cuprous oxide (Cu_2O). While both are important (and both will be discussed), cuprous oxide memristors are of special interest as this is the material that will be used on the copper spheres.

Work has been performed at AFIT to demonstrate the memristive capabilities of a $Cu/Cu_2O/Cu$ system [4]. In his Masters thesis, Castle deposited a 100 nm layer of copper on a silicon substrate. Copper oxide layers were grown using a quartz tube furnace. The copper oxide layers, which were no greater than 100 nm, were used to conduct electrical testing. The hysteresis in the I-V curve trace indicated the memristive behavior of the copper oxide system. Figure 2.9 is an I-V curve measurement of Castles memristive system.

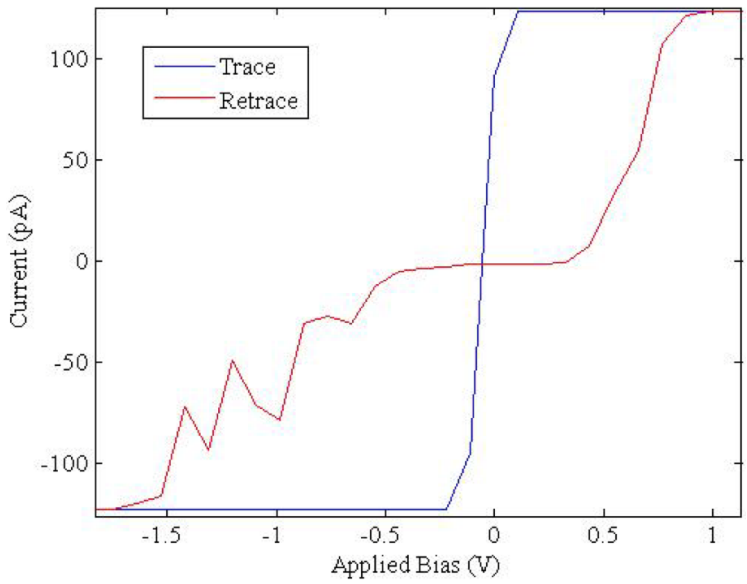

Figure 2.9: Hysteresis loop measured by Castle for his thesis, which demonstrated the memristive capabilities of copper oxide [4]

In general, Castle's data agrees with other work done on copper oxide devices. It can be seen by Figure 2.9 that the Cu_2O system behaves with a bipolar switching mechanism, implying a field-dominated operation. Castle noted that his results demonstrated similarities to the results of Dong [4, 10]. Dong speculated that the behavior may possibly be attributed to the migration of copper ions, though stated that the dominant mechanism could not be confirmed [10].

By contrast, not all research on copper oxide memristors has revealed bipolar resistance switching. Using a planar substrate and a micron-scale device, Fujiwara demonstrated the electroforming process as well as a nonpolar switching mechanism in CuO [11]. After an electroforming process, the device would reach a low resistance state. After several voltage ramps of the same polarity, the device would then switch to the high resistance state at 6 V. The set from the high resistance state to the low resistance state would then occur at 12 V. It is important to note for this research, however, that the devices were very thick compared to typical memristive devices - perhaps too thick to

observe bipolar switching. Since bipolar switching depends strongly on the ionic drift caused by an electric field, the nano scale range of drift induced on a device with micron-scale thickness would be relatively unnoticeable. McDonald performed tests on an Al/Cu_xO/Cu device and found bipolar and nonpolar characteristics [25]. These devices had a thickness much less than what was used by Fujiwara. Their results indicated that their switching mechanism could be due to a voltage-driven filament composition modulation rather than the more popularly suggested Joule-heating mechanism. Lv also made use of an Al/Cu_xO/Cu device [23]. Lv used a metal/Cu_xO/Cu device to test for endurance improvements between 3 metals as the top electrode: Ti, Pt, and Al [23]. Testing each device, it was found that the Ti TE exhibited almost no switching mechanism while the Al TE demonstrated excellent switching. Their results showed that an Al top electrode developed a layer of AlO_x, which aided in the switching mechanism. The Al and Pt devices exhibited bipolar switching, which was attributed to the drift of oxygen ions or vacancies through the conductive channel. However, their devices also demonstrated nonpolar switching, which they speculate is due to chemical reaction in addition to Joule-heating.

It seems that copper oxide may have potential for bipolar and nonpolar switching mechanism [23, 25]. Perhaps certain attributes of the copper oxide memristive behavior went unobserved for particular focuses in research. These pieces of research indicate a strong potential for copper oxide memristors.

2.7 Summary

Research in memristor technology is relatively young and still in the process of being fully understood. While many aspects of memristors are not yet fully understood, particular aspects of memristors are well established. The materials and processes that are used to build memristors have been used repeatedly to demonstrate a variety of behaviors that have been found in memristors. A general pattern that has emerged is the use of a thin

layer of a metal oxide with ohmic contacts. These particular traits of widely studied memristors will provide a background and rationale for researching cuprous oxide memristors on a spherical copper substrate.

III. Methodology

3.1 Chapter Overview

The purpose of this chapter is to explain the experimental processes that were used to investigate the 1-dimensional array of spherical cuprous oxide memristors. This section explains the processes that were used to gather information on the surface characteristics, the processes that were used to improve the surface characteristics, and the electrical measurement process and experimental setup.

3.2 Structural Evaluation of Copper Spheres

The copper spheres were distributed by Industrial Tectonics Inc. and manufactured by Canfield Technologies using a proprietary fabrication method. Per specification, the spheres were fabricated with copper to be 600 μm in diameter. Copper was selected because of its excellent electrical properties as well as its availability as an inexpensive commodity. Additionally, it has been shown that copper and its natural oxides exhibit memristive behavior [4, 10, 25]. As a preliminary step in characterization, the spheres were analyzed for their size, structure, and surface characteristics. The size is important for preparing further portions of the experiment as well as having a knowledge of the volume of copper. Knowledge of the atomic structure may be helpful for fully understand the spheres' conductive properties. Finally, surface characteristics such as roughness and grain size were analyzed to observe and compare the oxidation results with past work performed by Castle [4]. These characterization methods will provide an insight for electrical characterization later in this research.

3.2.1 Measurement and Imaging Using a Scanning Electron Microscope

In order to measure size, specifically, the radius and how it varies among spheres, an image of the entire sphere must be taken. Using a Scanning Electron Microscope (SEM),

clear images can be taken with micron-scale resolution. An SEM creates an image of a sample by emitting electrons from a field-emission gun onto a sample and detecting the Secondary Electrons (SEs) or Back-Scattered Electrons (BSEs) that are then emitted from the sample.

When the gun emits electrons, an accelerating voltage ranging from 1-40 kV is applied to the electrons [21]. The electrons are then focused through several electromagnetic lenses, which can be adjusted for achieving a focused image. Once focused through the final lens, the electrons strike the specimen, resulting in elastic or inelastic scattering. These different types of collisions produce different types of electrons from the sample: backscattering electrons and secondary electrons, respectively. The electrons produced as a result of collision from the emitted electrons are used to image the sample by a detector. The lower energy SEs are pulled into the detector with a bias voltage. The BSEs, however, have a much higher energy and must travel directly into the detector. Figure 3.1 shows a schematic of how these electrons interact with the sample.

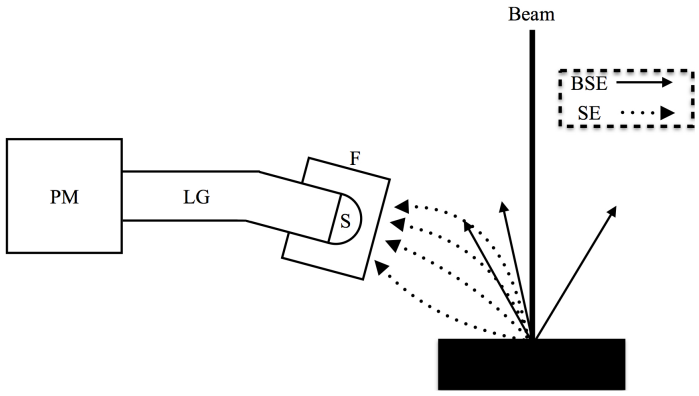

Figure 3.1: A simple depiction of SEs being drawn into the detector. As the electron beam strikes the samples, high-energy BSEs will reflect back toward the beam while low-energy SEs reflect and are attracted toward the detecter with an applied bias. Electrons enter the scintillator (S) and are converted to photons, which are then sent through the light guide (LG) and into a photomultiplier tube (PM) where photons are amplified and displayed. Adapted from [21].

Once the electrons are in the detector, the signal is converted to photons, which travel through a light guide, enter a photomultiplier tube, and are finally amplified to be displayed on a digital screen [21]. The digital screen can take image-averaged photos that are used to view the specimen with reduced random noise. The SEM images were produced from emitted electrons with an accelerating voltage of 5 kV. The images were produced primarily from SEs, which are useful for producing surface images.

3.2.2 Surface Characterization Using Atomic Force Microscopy

Measurements with Atomic Force Microscopy (AFM) will provide a nanometer-scale resolution image of a samples surface using near-field forces to generate a topographical image. AFM works by using a very sharp probe tip which is used to scan across the surface of a sample [21]. During the scan, the cantilever on which the probe tip is located senses the near-field forces between the probe tip and the sample surface. Atop of the cantilever is a thin metal coating, which reflects a laser onto a photodiode near the sample stage. When the forces along the surface cause deflection in the cantilever, the laser moves with respect to cantilever and thus its position is changed on the photodiode. This displacement can be sensed to a high degree of accuracy. With the elastic properties of the cantilever known, it is possible to calculate the forces between the probe tip and the surface based on the amount of deflection in the cantilever. Figure 3.2 is a schematic of AFM as described above.

Using contact mode of the AFM, the surface of the copper spheres can be imaged. These images can then be analyzed in Nanoscope, a software interface that allows for a wide range of AFM data analysis and imaging. As previously mentioned, the copper spheres have only been exposed to air, meaning the oxidation may be very uneven and will likely need to be etched and regrown.

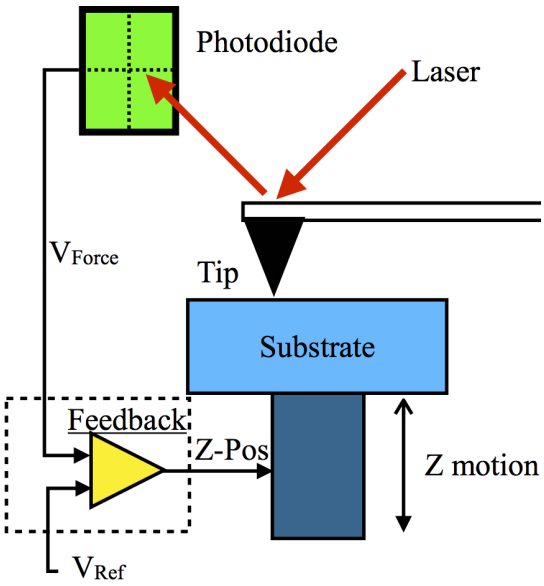

Figure 3.2: This schematic depicts the functionality of the Atomic Force Microscope. As the AFM tip moves over the surface of the substrate, verticle surface features cause the cantilever to bend, which then moves the laser from the center of the photodiode. The position of the laser on the photodiode is calculated into a force and signaled to the feedback loop, which adjusts the verticle position of the stage. Adapted from [55].

3.2.3 Structure and Lattice Analysis Using X-Ray Diffraction

The structure of the copper spheres can play a large role in the electrical and mechanical properties. A particular crystalline structure could affect the conductivity and Young's modulus depending on crystal orientation and the direction of grain boundaries. If this were the case, the use of tensors would be critical in calculating basic device parameters. By performing measurements with an X-ray Diffractometer (XRD), it is possible to learn about the structure of a sample as well as some basic clues about the composition. An XRD is a method of diffractometry that bombards X-rays onto a polycrystalline sample [21]. The X-rays are then continuously diffracted from the sample in all directions. A detector moves in a half-circular motion around the stage of the sample and detects the intensity of X-rays that are being diffracted a certain angles from the sample. Figure 3.3 is a simple depiction of how the X-rays are diffracted from the sample.

Once the X-rays are detected, they can be plotted to show at which angles their intensities were greatest.

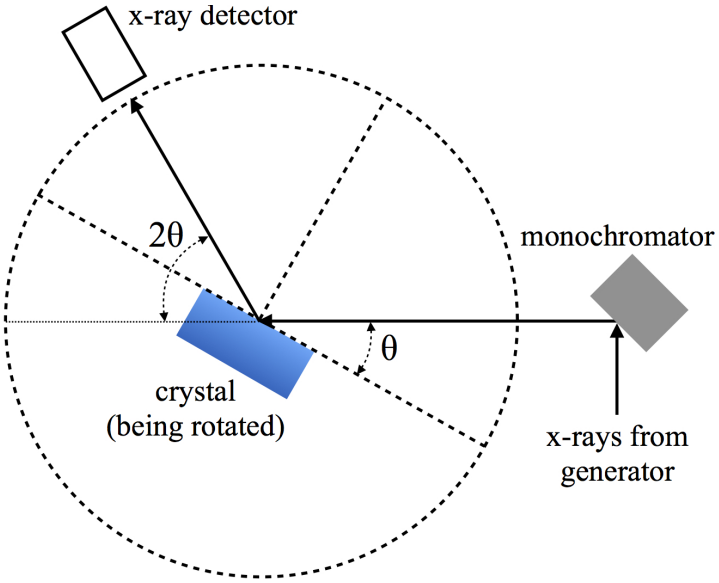

Figure 3.3: Operation schematic of and XRD. After X-rays are generated from the anode, they are bombarded onto the sample. Adapted from [21].

The patterns of detected X-rays show at which angles the X-ray diffractions are most intense. These patterns are unique to different materials. A database which stores all the XRD patterns of a nearly all polycrystalline materials can be used to match the measured XRD pattern to one in the database, making it possible to identify an unknown material, or perhaps identify a secondary material that may be an impurity in a primary material. Using this method with the copper spheres as test samples, it will be possible to confirm that the spheres are copper as well as identify their atomic structure. Additonally, an XRD measurement can identify if any strain exists in the Cu_2O layer. Figure 3.4 shows the known XRD patterns of FCC copper and cuprous oxide. These plots serve as a good demonstration of what will be expected. If the spheres are composed of copper and

possibly consist of a native oxide layer as expected, the measured XRD pattern will be a combination of these plots.

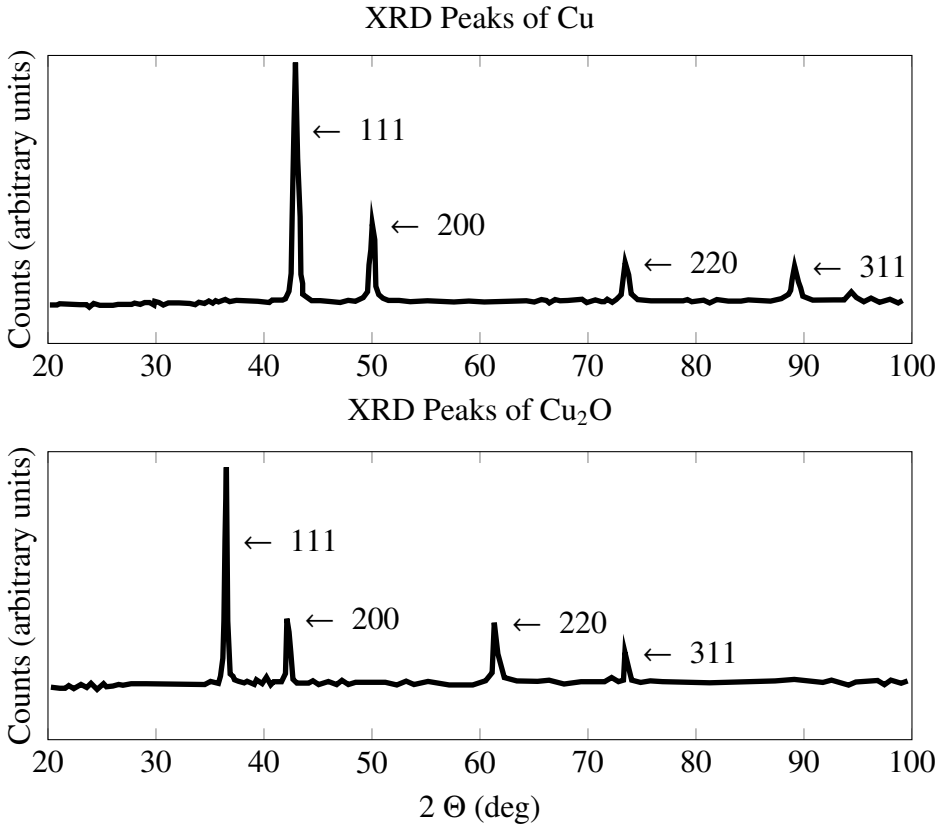

Figure 3.4: Characteristic XRD peaks of copper and cuprous oxide. When FCC copper and cuprous oxide are characterized using XRD, the plots that occur are as shown here. The characteristic peaks of these plots are what is expected for the XRD pattern of the copper spheres. Data from [45].

Before taking diffraction measurements of the copper spheres, the XRD was set up with specific parameters. The equipment used was an XPERT-PRO Diffractometer and High Score material database software. About 50 copper spheres were placed on a tape surface, which held the sample in place when it was raised perpendicular to the floor. The diffractometer was set up with a copper anode, which ejected K-alpha waves with wavelength 1.542 Å. The generator voltage was set to 45 kV with a 40 A current. A

scanning range of 20-120°along a 2-theta angle was used because the expected first peak was around 35°. During the 90 minute scan, 4999 data points were taken. Using this data, it will be possible to learn about the structure and composition of the spheres.

3.3 Copper Sphere Surface Preparation and Fabrication

The as-received copper spheres had a native oxide layer that may have developed in the presence of unknown contaminants and loose debris on the surface. In order to build a standard device and minimize variation between spheres, an etching and oxidation process was used to prepare the copper spheres for electrical testing. The etching processes were performed with liquid phase etchants and was used to produce a cleaner sphere surface. The oxidation processes each produced nanometer-scale surface oxides that will serve as the memristive sphere-to-sphere interface.

3.3.1 Surface Cleaning and Polishing by Acidic Etching

A prerequisite to growing a new oxide layer is the removal of contaminants and debris. The spheres can be cleaned and polished using acids to etch the surface, achieving a clean, polished surface. The copper spheres were etched with two etchants in order to compare their success. The first etch involved the use of an organic acid. Chavez showed that various forms of copper oxide could be etched with acetic acid [5]. Acetic acid is a very effective etchant for removing copper oxide in any of its oxidation states. The etching process is a chemical reaction between copper oxide and acetic acid resulting in the formation of copper acetate and water. When etching cuprous oxide, the reaction also forms hydrogen gas, as shown below [5]:

$$Cu_2O + 4CH_3COOH \rightarrow 2Cu(CH_3COO)_2 + H_2O + H_2 \tag{3.1}$$

The etching process followed very specific steps to ensure a safe use of chemicals. The spheres were sonicated in a 50 mL vial with 2 mL of acetic acid for 10 minutes to ensure a uniform etch. After etching, the copper spheres were rinsed in deoxygenated

water and dried. Figure 3.5 shows the experimental set-up for etching the copper spheres with acetic acid.

Figure 3.5: The experimental setup for performing the acetic acid etch of as-received spheres. The as-received spheres are placed in a 50 mL vial with 2mL of glacial acetic acid. Placed inside a larger beaker to maintain a verticle posture, the system is placed in a sonicator to ensure a uniform etch.

The second etching process uses an inorganic acid. It has been shown that diluted nitric acid can perform well as an etchant for copper oxide [42]. In his experiment, Toth used nitric acid in a 1:1 mixture with water to clean the surface of oxidized copper [40]. It is especially important to dilute the nitric acid in at least a 1:1 mixture when etching copper oxide. Nondiluted nitric acid reacts in an exothermic reaction with copper, shown below.

$$Cu + 4HNO_3 \rightarrow Cu(NO_3)_2 + 2NO_2 + 2H_2O \tag{3.2}$$

The result is a formation of brown toxic gas called nitrogen dioxide. By diluting the nitric acid in water, the exothermic reaction is inhibited due to the chemical reaction shown below.

$$3Cu + 8HNO_3 \rightarrow 3Cu(NO_3)_2 + 2NO + 4H_2O \tag{3.3}$$

During the etching process on the copper spheres, nitric acid was diluted in water an 80:20 (H_2O:HNO_3) mixture inside of a 250 mL beaker within a hume hood. The spheres were deposited into the etchant and sonicated for 5 minutes. After the etch, the spheres were rinsed with DI water to remove any traces of nitric acid. The spheres were allowed to dry in an open air environment until it was clear that there was no moisture among the spheres, which was indicated by the spheres no longer sticking together in a way that is similar to wet sand. Afterwards, the spheres were imaged in an SEM to observe the effects that the etch had on the sphere surface.

3.3.2 Thermal Oxide Growth Processes

Once the native oxide layer is cleaned and polished, the copper surface of the spheres are ready to grow a new oxide layer. Copper oxidizes very easily in normal air and develops at a different rate depending on the temperature and pressure. It has been shown that in normal air at room temperature, copper grows a native oxide that could be between 3 to 5 nm in thickness over a 48 hour span [16]. Roland indicates that at 100°C, the thickness of copper oxide develops at a rate

$$d^3 = 0.86t \tag{3.4}$$

in which d is the thickness in nanometers and t is the time exposed to the heated environment in seconds [3, 39]. This equation was used to approximate the thicknesses, shown in Table Table 3.1, that may be achieved at selected amounts of time to grow varying thicknesses.

The values for Equation (3.4) compare well with relationships formulated by Matsumura [24]. Matsumura used thermal dry oxidation in low temperatures (below 350 °C). Their results allowed the formulation of equation that describes the thermal oxidation of Cu to form Cu_2O and is shown below in Equation (3.5).

$$d^2 = 1.35 * 10^7 t_{ox} e^{\frac{-0.97}{kT_{ox}}} \tag{3.5}$$

In Equation (3.5), d is in μm and t_{ox} is in minutes. This equation also holds a third term, accounting for the temperature T_{ox} in which the oxide was grown in Kelvin (K).

Table 3.1: Oxidation times and estimated thicknesses using Equations (3.4) and (3.5). These oxide thicknesses are the result of oxidation at 100°C. Both experiments involved the use of a dry O_2 gas flow at atmospheric pressure.

Oxidation time (min)	Est. thickness (nm), Eq. 3.4	Est. thickness (nm), Eq. 3.5
1	4	1.0
5	6.4	2.3
15	9.2	3.9
30	11.6	5.6
60	15	7.9
120	18.4	11.3

As the data in Table 3.1 indicates, the oxidation of copper is a slow process. As Campbell's data shows, the first few nanometers grow quickly; however, it takes roughly 15 minutes to double the thickness after the first minute of oxidation; and then another 105 minutes after that to double again. Data from Matsumura shows that the oxidation process occurs much slower, but remains on a comparable scale. These estimations were used to select which oxidation times would be used for the oxidation of the copper spheres

based on the best variability that may be found in the electrical characterization process. At the same time, it is important to achieve a thickness in the right range. For example, the oxide thickness must be at least thick enough to ensure that the entire sphere surface has developed an oxide. The oxide that grows on a copper surface develops in a spotty pattern, meaning for some thickness of oxide development, there may still be areas on the copper surface that has not yet developed an oxide. Additionally, the oxide thickness must be such that it can withstand external forces such as those from an adjacent sphere pressing against it. By contrast, the oxide layer must be thin enough so that memristive behavior can be observed.

3.3.2.1 Thermal Oxidation in a Quartz Tube Furnace

In order to perform the oxidation process, the copper spheres were loaded into a pipette and allowed to spread out such that no spheres were stacked above other spheres. A gas mixture of 50/50 oxygen and argon was allowed to flow through the pipette and over the copper spheres. This gas mixture was used because it was shown to successfully produce memristive effects as shown by Castle [4]. The pipette was placed inside a quartz tube furnace that held a temperature of 100°C. Assuming mass transfer limited growth, the pipette was rotated 90° every time one-fourth of the oxidation time passed, helping to ensure a uniform oxide growth. This meant that for the 1 minute oxidation, the pipette was turned every 15 seconds and for the 2 hour oxidation, the pipette was turned every 30 minutes.

The oxidation times for 1 minute, 15 minutes, and 2 hours were chosen for their prospective thicknesses, which seem to double at each interval of time. Additionally, the 5 minute oxide was selected to observe how smaller changes in thickness effect overall characterization. In addition to these oxide thicknesses, a separate set of spheres was oxidized for 120 minutes at 200°C. Cambell and Thomas show that at 194°C, the rate of oxidation for copper is about an order of magnitude greater than when the temperature is

100°C [3]. Such a rate would provide a thickness estimation of about 180 nm for the oxidation at 200°C. A value on a similar scale is found using Equation (3.5), estimating a thickness of about 270 nm.

3.3.2.2 Thermal Oxidation in Air on a Hot Plate

In addition to the more controlled process of oxidation in a furnace, interest arose in developing a native oxide in a normal air environment. This could be done quickly and simply by allowing the spheres to oxidize in an open air environment upon hot plate. In order to build a native oxide in normal air, some sets of spheres were oxidized in an open air environment on a hot plate. Because of the less-controlled circumstances of this oxidation method, a planar copper sample was simultaneously oxidized to observe the surface roughness of the resulting oxide layer using AFM so it can be later compared to the roughness data that was gathered by Castle in using a quartz-tube furnace [4]. The planar copper samples are identical to those used by Castle. They consist of an electroplated gold layer upon a silicon substrate. Upon the gold layer, copper is evaporated into a 100 nm thin-film. This copper thin film would build into a non-crystalline structure, which is similiar to the copper spheres and will serve as a good planar comparison to the oxide growth on the spheres.

The spheres and planar copper samples were set in a petri dish which was covered to prevent room-temperature air from circulating over the hot plate. Inside the petri dish, a temperature sensor was taped to the plate to monitor and verify the temperature of the hot plate was maintained at 100°C. The spheres were then oxidized for 1, 5, and 15 minutes and moved around inside the petri dish every 20-30 seconds to help achieve a uniform oxide growth around the surface of the spheres.

In addition to these oxidation processes, a fourth hot-plate oxidation process was done to observe the oxidation of the spheres when no etch has been done to clean the sphere surface. This set of non-etched spheres were oxidized in an uncovered hot plate for

5 minutes. The spheres were left uncovered for this oxidation in order to observe the effects on roughness by comparing the planar copper samples from each set. There were no 1-minute or 15 minute oxides for the uncovered set because such time dependent variables would be redundant.

3.4 Experimental Setup for Electrical Measurements

The data acquisition setup was very similar for each data set. In general, there was a single containment method for holding the spheres in a linear position and compressing them. For the electroforming and basic electrical characterization, there was a stage that allows for basic manual adjustment to supplement the compression level of the spheres. For testing the electrical response to physical compression, a more precise computer-controlled stage was used to provide a measured displacement. The displacement can then be translated by calculation into a value of applied compression force. Measurements were conducted on each of the four oxide-thicknesses that have been grown on the spheres. These data provide an insight to how the memristive interfaces behave in general and how processes that were used to build them can vary the behavior.

3.4.1 Sphere Containment Apparatus and Circuit Connections

In the experiment, the spheres were contained within an optically transparent glass tube that has 700 μm-wide openings on each end. Blocking each end will be a 680 μm-diameter conductive rod made of high-purity (99.95%) tungsten. The rod on one end will be fixed within the tube to withstand axial forces and the rod on the other end will be positioned upon a V-shaped stage, which will hold the glass tube in a tight, immobile position. Figure 3.6 shows the experimental set up.

The spheres can be compressed in two ways. The manual-controlled method involves using a Thorlabs T12X movable stage that compresses the spheres by 250 μm per full crank rotation while the computer-controlled stage is held still. The other way involves the

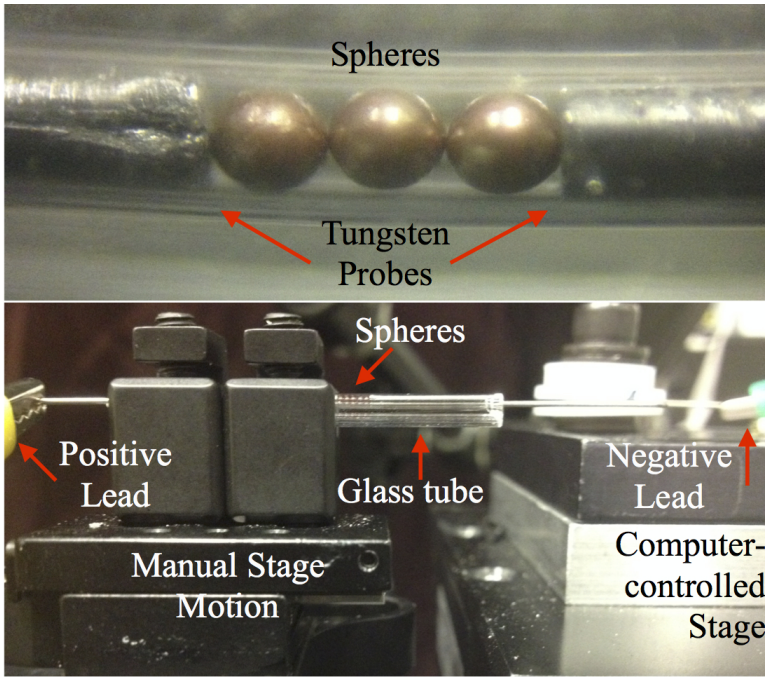

Figure 3.6: The experimental set up involving the sphere containment tube and circuit connections. The glass capillary tube is held upon the left manual-motion stage and has a tungsten rod fixed within the left side of tube. The tungsten rod on the right side is fixed upon the computer-controlled stage and can move freely within the glass capillary tube as the manual-controlled or computer-controlled stages are moved. Each tungsten probe acts as an electrical lead, connecting the spheres in series with the source and measurement system.

use of an Aerotech ANT 130-XY computer-controlled micromanipulator, which can compress and read displacements with nanometer accuracy while the manual-controlled stage is held still.

For each measurement, the tungsten rod was used to compress the spheres within the glass tube in order to apply an axial force. When the rods pushed all the spheres in contact, an electric potential was supplied to the copper sphere chain from electrodes that are in contact with the tungsten rods. To ensure the tungsten rods do not compromise the accuracy of the current-voltage measurements, the measurement system was tested on the

0-sphere system. Figure 3.7 shows the resistance of the tungsten rods when in direct contact to each other.

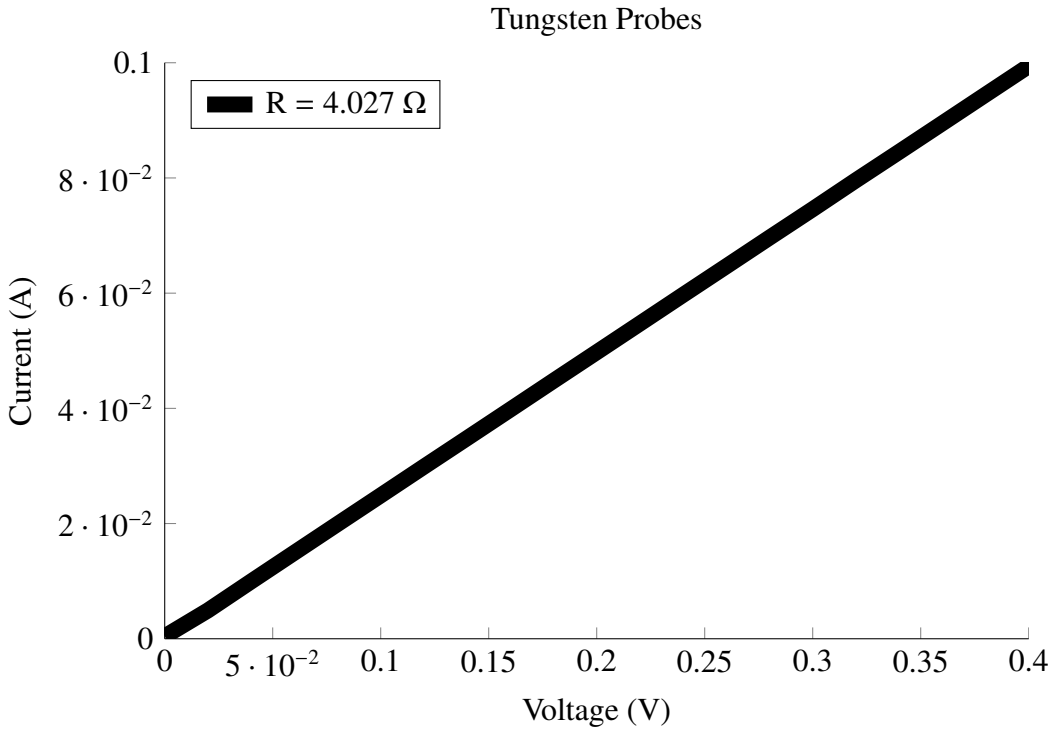

Figure 3.7: The I-V curve for the tungsten rods. This data shows that the resistance of the system without the spheres is 4.026 Ω. This resistance is insignificant when compared to that of the spheres which have resistances in the MΩ range.

The method of measurement involved sourcing voltage and measuring current. The potential was supplied directly to the tungsten rods with the positive lead on the left side and the negative lead on the right side as shown in Figure 3.6. The negative lead is connected to the high signal end of the measurement lead. This connects in series with the ammeter and the low signal connector, which connects to ground. The circuit schematic is shown in Figure 3.8.

Electrical measurements were performed using a Keithley 6517A Electrometer. The measurements were controlled and recorded via LabVIEW by communicating a voltage

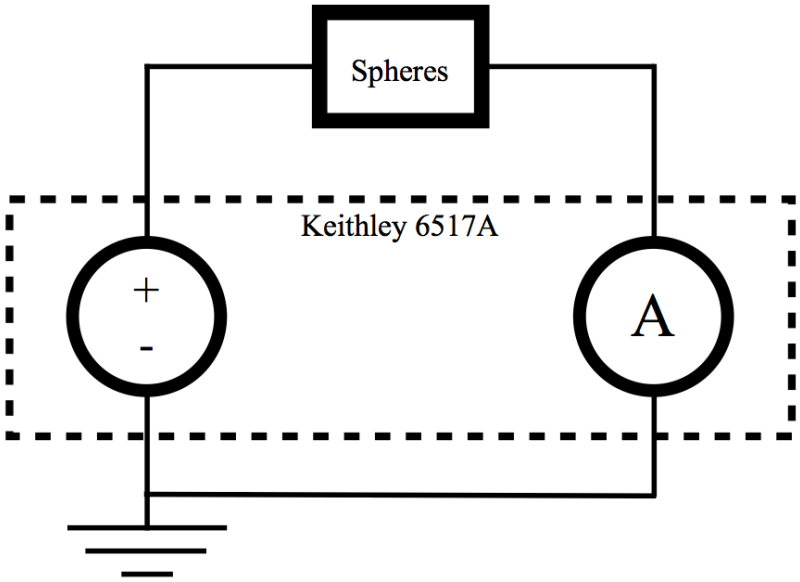

Figure 3.8: This schematic details the circuit connections for taking current-voltage measurements. The Keithley 6517A sources a voltage, which is applied to the spheres. The low-end of the spheres is connected to the high-end current measurement lead. Finally, the low-end current measurement lead is connected to the ground along with the negative source lead.

value to apply and recording the resulting current. Accordingly, the Keithley 6517A would receive the information from LabVIEW, apply a voltage, and measure the resulting current. This information is then communicated back to LabVIEW and recorded.

3.4.2 Nanopositioner for Precise Compression of Spheres

In order to collect data when testing the electrical behaviors against mechanical deformation, a computer-controlled stage is used to provide a more accurate compressional motion. The computer-controlled stage provides measurable, precise motion that is accurate to ~1 nm. Each oxidation-type experienced the same levels of compression to test for each spheres' sensitivity. These compressive displacements increased by 10 μm. After forming an electrical contact, an I-V curve was collected. This was done until the spheres reached an amount of compression that saturated the memristive interfaces of the spheres and brought the spheres to an ohmic behavior.

This experimental setup provided a well-controlled, repeatable means of demonstrating the device characteristics of the spherical copper oxide memristors. Ultimately, the experiment tested the characteristics of what may be used as a system protection sensor. This fact emphasizes the importance of collecting data that demonstrates that the devices behave in a way that is repeatable.

3.5 Electrical Characterization and Data Acquisition

Characterizing the electrical behavior of the spherical copper oxide memristors required 3 steps in measurements. First the devices will needed to experience an electroforming process. Next, the spheres I-V curves were characterized while compressed to a minimal electrical contact in order to understand the devices without interferences. Finally, the I-V curves of the spheres were measured while a compressive force was applied to the system.

3.5.1 Electrical Measurements

In order to gather meaningful data for a memristor, it was necessary to electroform the device. The electroforming process creates a conductive path in which the motion of ions changes the resistance within the conductive path. While performing the electroforming process, a voltage sweep was be applied for a range of values starting from 0 V.

Once the spheres were electroformed, they were ready to be characterized by their I-V curves. Using the same electrode placement for applied voltage and current measurement, a voltage sweep was applied from 0 to V+, then from V+ to V- and back to 0 V. This trace provided a full view of electrical behavior involving the current-voltage relationship.

A strong understanding of the devices is built by performing these measurement steps before collecting data on the electrical response to mechanical deformation. First, by electroforming, the spheres are morphed into a conductive state and are more responsive

to voltage signals. Second, by characterizing the basic electrical properties, a good voltage range for conducting measurements can be found. It is preferential to conduct measurements with a lower voltage because it shows that the devices can perform with low power consumption and may potentially endure a greater range of compression. When under compressional stress, increased contact areas will result in lower resistances, which will cause the current to increase. The increased current may potentially cause the sphere to experience a complete dielectric breakdown at a voltage lower than is usually experienced when under no compressional force.

3.5.2 Electrical Testing Under Applied Force

Once the copper spheres were characterized for basic electrical properties, mechanical stress was tested against their electrical behavior. In order to do this, a similar stage set up held the spheres in place while a motorized, computer-controlled stage was used move a tungsten rod in toward the spheres to induce compressive forces on the spheres that went as high as 100 mN.

The electrical properties were tested while inducing varying levels of compressive force. At each interval of compressive displacement, an I-V curve was traced. This process of data acquisition was repeated until just before the oxide on the spheres reached an operating limit which may either be complete dielectric breakdown or a state of plastic deformation. This breaking point occurred in each sphere type at different levels of compressive displacement, depending on the respective oxide thickness and the number of spheres being tested.

Using the data gathered in this experiment, a map can be created that shows how the electrical behavior of the spherical copper oxide memristors changes when mechanical stress is applied. With this technique, 3 dimensions of data are collected. These dimensions are voltage, current, and applied force. With these data, a 3-dimensional plot can be created to show the gradual changes that occur in the I-V curve of the system.

As Chapter 4 will show, these data are evaluated for their repeatability. By finding a system that is reproducible in nature, it will be possible to depend on certain data when proceeding to higher dimensions of testing spherical memristive systems.

3.6 Summary

This chapter explained the steps of processing and electrical testing for characterizing the spherical copper oxide memristors. The three major steps in fully characterizing the spheres involves building a memristive copper oxide surface, electroforming and basic electrical testing, and mapping changes in electrical behavior to increasing amounts of mechanical stress.

IV. Results and Analysis

4.1 Chapter Overview

This chapter presents the results of this research and provides discussion on data interpretation. The discussion first goes into the findings of the material, physical attributes, and structure of the copper spheres. Next the chapter will discuss the results of the etching and oxidation processes and clarifies the process that was used to implement the main electrical tests. Finally, this chapter will discuss the results of the current-voltage relationships found in the cuprous oxide spheres and their changes in electrical behavior with physical interference, which results in memristive behavior that is shown to provide sensor capabilities.

4.2 Physical and Structural Characteristics of Copper Spheres

The results provided in this section reveal practical information that was needed in order to plan this research and future experiments. It reveals insights to geometrical parameters and qualitative information on the surface quality of the spheres.

4.2.1 Diameter Measurements and Imaging using SEM

Basic information on the dimensions and features of the spheres was able to be gathered using Scanning Electron Microscope (SEM). As received by the manufacturer, the copper spheres appear with a textured surface. Figure 4.1 shows the SEM image of a single copper sphere including a diameter measurement of 684.1 μm. This image clearly demonstrates that the rough, flakey surface appears on the micron-scale, indicating that these surface textures result from the copper metal that makes up the bulk of the sphere.

In some parts of the spheres, such flaking is more pronounced, causing surface anomalies as indicated in Figure 4.1, which provides a zoomed image. This specific

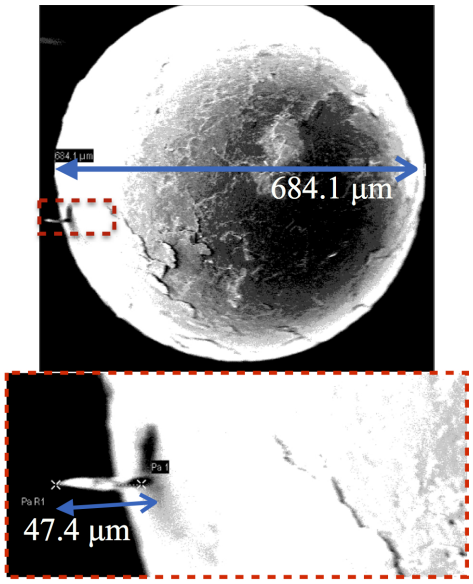

Figure 4.1: The SEM image of the copper sphere surface and a zoomed view of emphasizing the flaking feature on the surface. These images depict just one sphere to demonstrate the surface conditions of the as-received spheres. The surface flaking can extrude from the surface as much as 47.38 µm.

surface flake was measured to be 47.38 µm in length from the surface. Such defects can be problematic as Figure 4.2 indicates.

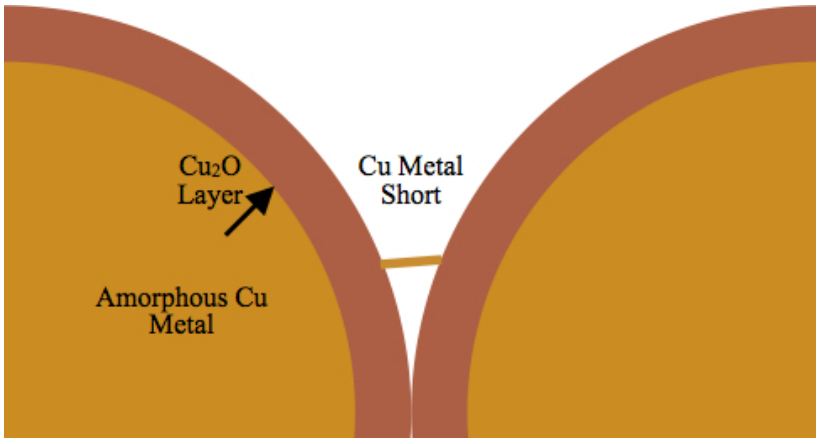

Figure 4.2: A 47 µm flake reaching between two spheres. Placed next to one-another, a copper flake extending 47 µm such as that shown in Figure 4.1 can result in an electrical short, which may compromise the accuracy of measurements.

The SEM images provide visual information about the surface texture as well as necessary measurements for the diameter and micron-scale surface features. The images indicate that the diameter is ~ 80 μm greater than expected. Additionally, the surface roughness that is visible in these images demonstrates the need for surface etching and oxidation processes. As Section 4.3.1 will demonstrate, the effectiveness of the etching processes are visible in SEM images.

4.2.2 Determination of Molecular Structure of Copper Spheres

Gathering structural material data on the spheres was an important step, as discussed in Section 3.2.3. An X-Ray Diffractometer (XRD) was used to gather this data. Shown in Figure 4.3 is the XRD pattern of the copper spheres. Upon observation, it can be immediately seen that the diffration pattern has an absence of peaks. This XRD pattern suggests the copper spheres have an amorphous structure.

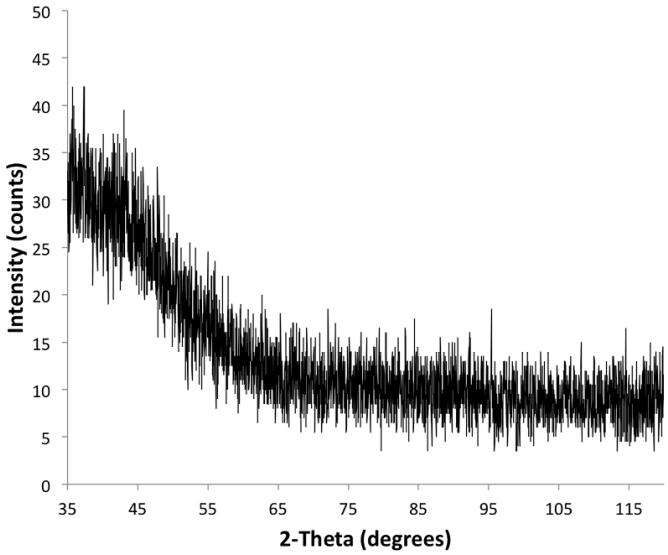

Figure 4.3: The XRD pattern shows the copper spheres to be amorphous in structure. The large hump at 35° may indicate that characteristic distances in the amorphous lattice may be on the scale of the lattice spacing on the typical Cu 111 plane which is 2.55 Å.

The amorphous structure can be used to infer certain aspects of the electrical behavior of the copper spheres. Johnson indicates that many amorphous alloys exhibit different engineering properties than their polycrystalline counterparts [11]. In many cases, material properties of amorphous metals have drastically changed [4]. If this is true, then this shows that it will be very necessary to conduct electrical tests on the copper spheres to discover specific electrical and material properties.

4.3 Surface Etching and Oxidation

The etching and oxidation of the copper spheres provided clear surface changes. The surfaces of the as-received spheres show very clear geography of cracks and are more metallic in appearance, indicating that any native oxide is very thin. After oxidation, the new surface oxide layer is clearly apparent as the spheres has a less metallic appearance.

4.3.1 Comparison of Effectiveness of Etches

The results of the acid etches varied significantly. While etches are usually compared by examining and comparing quantitative dimensions of an etch, these results are compared by visual surface effects and the subsequent electrical behavior. Upon visual observation of the spheres' surfaces, the acetic etched spheres appeared noticibly brighter, as Figure 4.4 shows. Comparatively, the nitric-etched spheres immediately developed a light native oxide layer, evident in their darker color.

Further imaging was done on the micron scale using SEM to demonstrate the clear surface changes. The smoother surfaces are evident in Figure 4.5 and can be compared to SEM images shown previously in Figure 4.1, which showed large surface debris and flaking. It can be seen here that the debris has been removed around the surface.

In addition to visual evaluation, the etching results were also compared by performing I-V traces to evaluate their electrical behavior. The expectation for these current-voltage measurements was to achieve a linear I-V curve, identical to a resistor

because the contacts between each sphere would ideally consist of copper. Below, Figure 4.6 shows the electrical behavior of freshly etched, non-oxidized spheres.

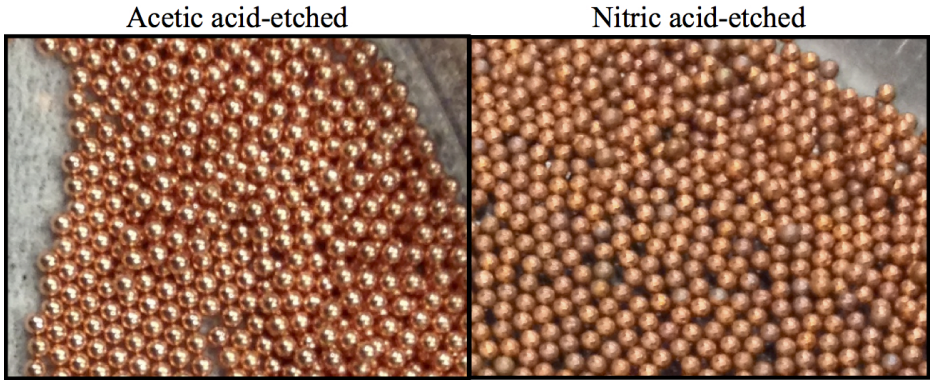

Figure 4.4: Photographs of the spheres immediately after their etches. Immediately after etching, the acetic acid-etched spheres have a brighter metallic shine. By comparison, the nitric acid-etched spheres are slightly darker, incidcating the presence of a native oxide.

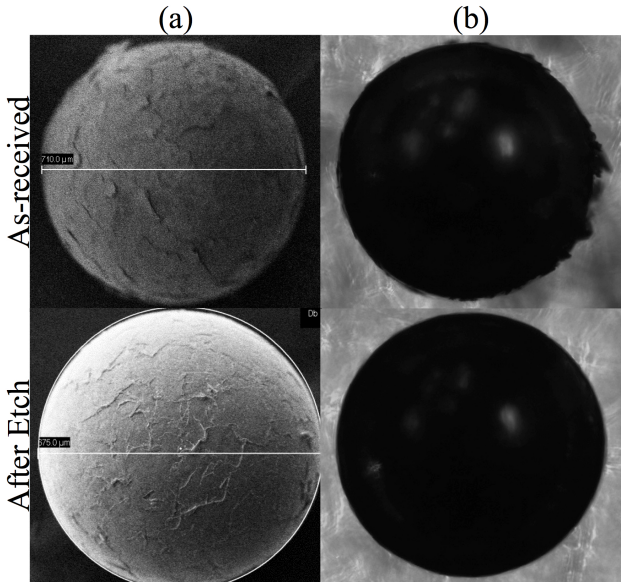

Figure 4.5: A comparison of etches before and after. On left (a) SEM image of spheres that have been etched with acetic acid. On the right, (b) microscopic images of spheres etched with nitric acid.

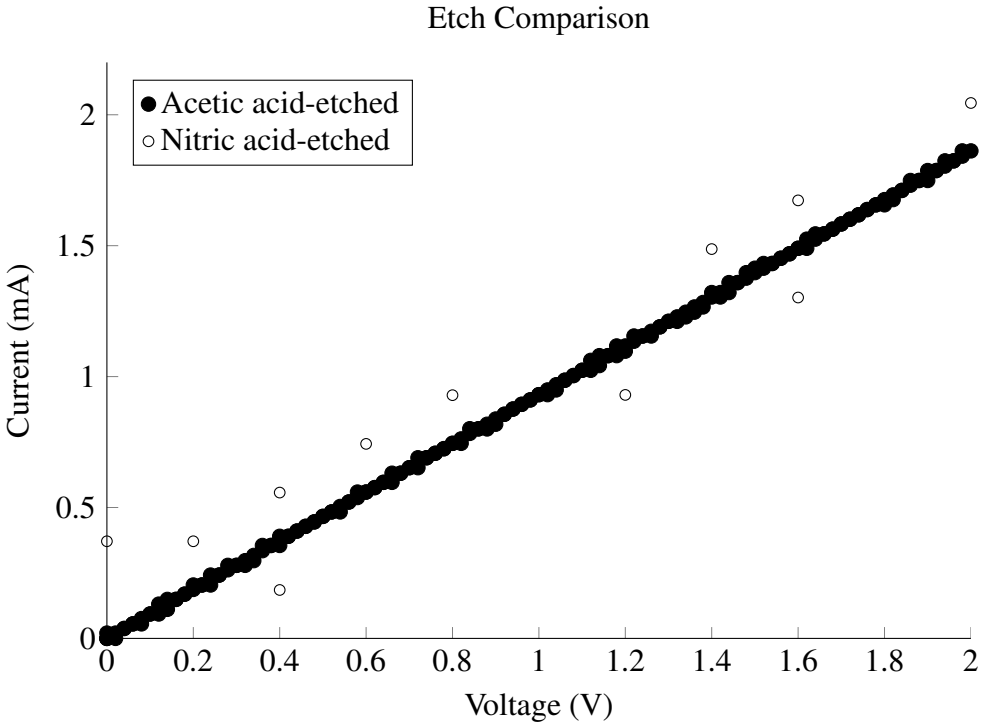

Figure 4.6: Comparison of I-V traces between the spheres etched with nitric acid and acetic acid. The data indicates that while both appear to provide an ohmic responose, the greater error in the nitric-etched spheres, which is on the order of 0.18 mA, suggest the presence of a thin native oxide layer.

The results of these I-V traces indicate that there was a slight difference in the etch results. While both spheres indicate an ohmic current-voltage relationship, as expected, there is noticibly more error in the data points of the nitric acid-etched spheres. This agrees with the information that was inferred by visual observation of the sphere surface, indicating that the nitric acid allowed a slight native oxide to develop over the copper surface. By contrast, it would seem that the coppper spheres etched with acetic acid did not allow much of an oxide to develop. This is discussed in the comparison shown in Section 4.3.2.

4.3.2 Comparison of Oxides

Freshly etched spheres were oxidized using two different processes for various lengths of time. The results of the oxides can be evaluated visually. As Figure 4.7 reveals, the effectiveness of the oxidation process depended on the etching process.

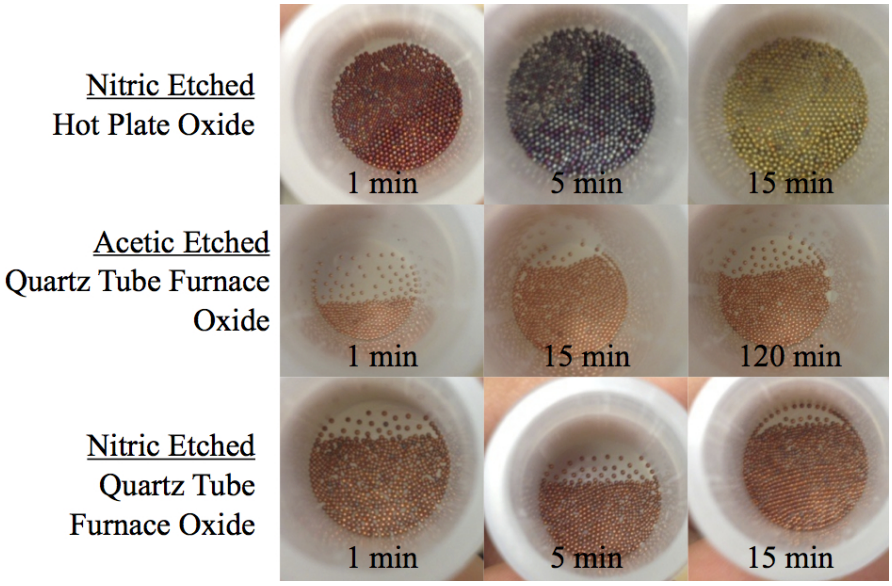

Figure 4.7: Visual comparison of spheres which underwent different etching and oxidation processes. These images show that the the greatest variation between oxidation times occurred using the hot-plate oxidation. By contrast, the spheres etched with acetic acid appear as they did after the etch.

The differences between the sets of spheres are very clear. As Figure 4.7 shows, the etching and oxidation processes both play a very critical role in the development of the final oxide layer. Specifically, the results show that the hot-plate oxidation using the nitric acid-etched spheres demonstrated the greatest changes in both visual appearance (as shown in Figure 4.7) and electrical behavior (which will be discussed in Section 4.4. In comparing the oxidation processes between nitric acid-etched spheres it can be seen that over time, the spheres oxidized in a quartz-tube furnace gradually develop a slightly darker orange surface and become less shiny. However, the acetic acid-etched spheres

seem to have remained the same through each length of oxidation, as evidenced in their color. Additionally, the oxidation results were compared by their electrical behavior. The spheres that were oxidized after etching with acetic acid appear copper-colored and comparable to their state before etching. Likewise, their electrical characteristics are captured in I-V curves. These behaviors demonstrate similar ohmic results as shown in Figure 4.6; aditional examples can be seen in Figure B.1. A review of the reaction in Equation (3.1) indicates that the products are cupric acetate, water, and hydrogen gas. This indicates that cupric acetate may have developed on the surface of the spheres that impedes the oxidation of the copper spheres.

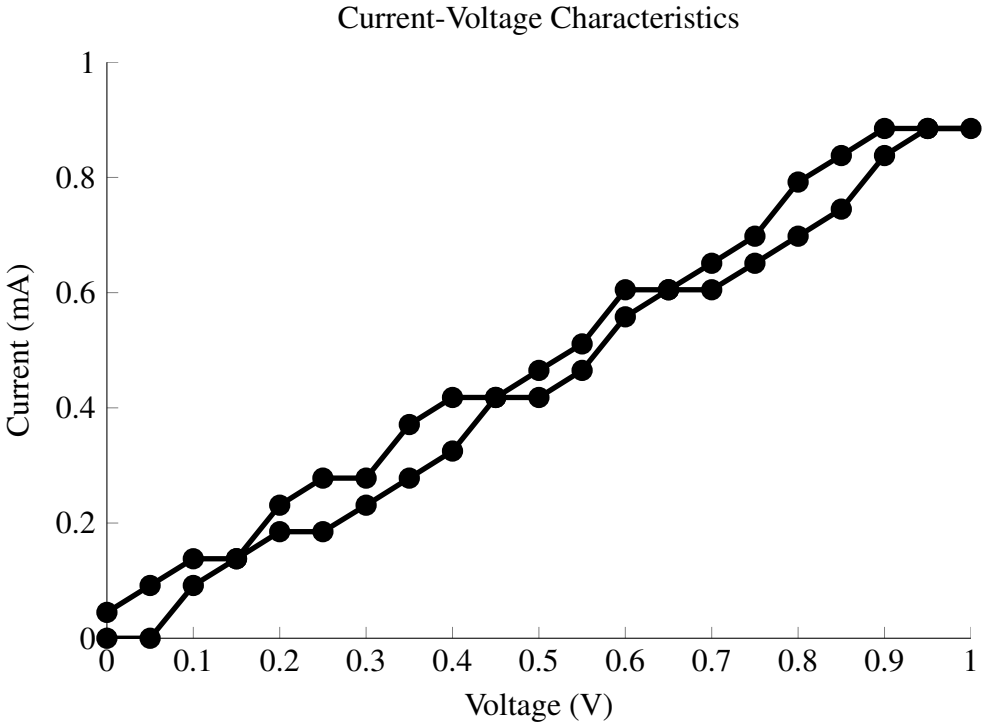

Figure 4.8: Representative example of the current-voltage behavior of the acetic acid-etched spheres. This curve shows the behavior of spheres oxidized in a quartz tube furnace at 100°C for 120-minutes.

The spheres etched with nitric acid and oxidized via Quartz-tube furnace demonstrate a more clearly grown oxide, however, inconsistent I-V characteristics for each of the oxide thicknesses made them difficult to repeatably measure. These can be seen in Figure A.2. As Figure 4.7 shows, the spheres etched with nitric acid and oxidized in a closed normal air environment on a hot-plate demonstrate the greatest changes from etch to oxidation as well as the transitions of oxide thickness over time, as described by the low-voltage I-V curves shown in Figure 4.9.

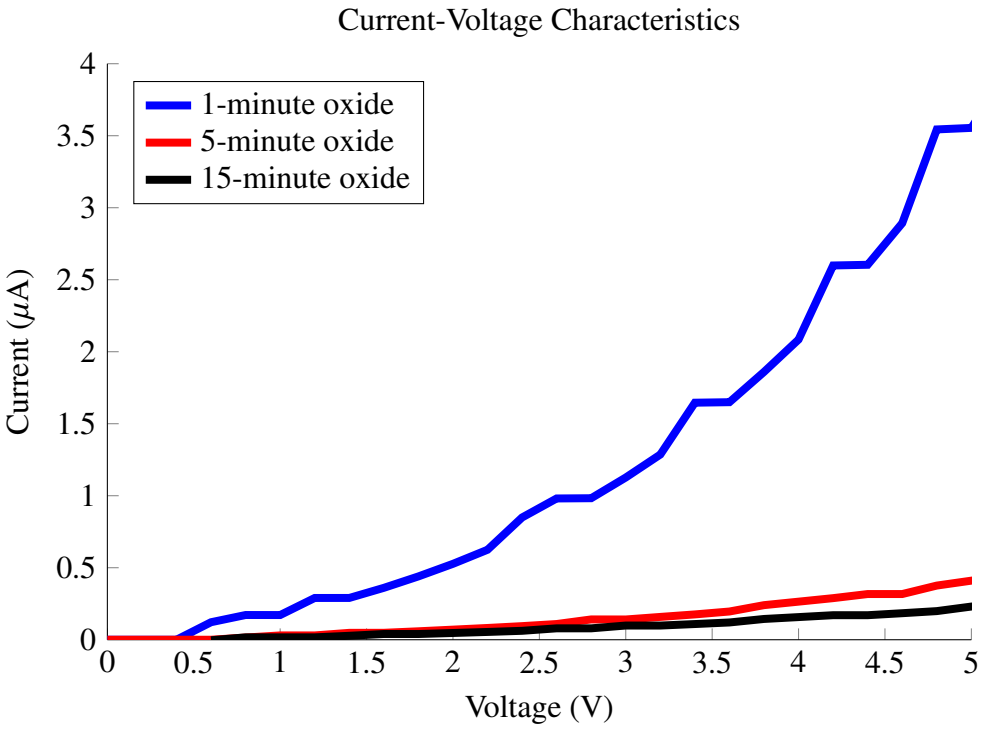

Figure 4.9: Representative example of the current-voltage behavior of the nitric acid-etched spheres that were oxidized on a covered hot plate in atmosphere at 100°C. We see here that the oxide thickness has an impact on the non-linear I-V behavior.

To maintain the organization of this document, these results are summarized here. Section 4.4.1 will demonstrate the electrical behavior of the spheres that were etched using nitric acid and oxidized on a hot plate.

4.3.3 Oxide surface characterization using AFM

The closed hot-plate system for thermally oxidizing the spheres provided a functional oxide layer; however, the process was relatively uncontrolled. Surface data gathered via Atomic Force Microscopy (AFM) was used to provide a comparison of this process to the process used by Castle [4]. During the thermal oxidation of the copper spheres, planar samples identical to those used by Castle were present in the environment. The planar samples are on a silicon substrate, which has been electroplated with gold, and sputtered with copper. Using these planar samples, data can infer qualities about the oxide surface on the copper spheres using AFM. In Figure 4.10, the AFM results for the planar copper oxide films for various oxidation processes are shown.

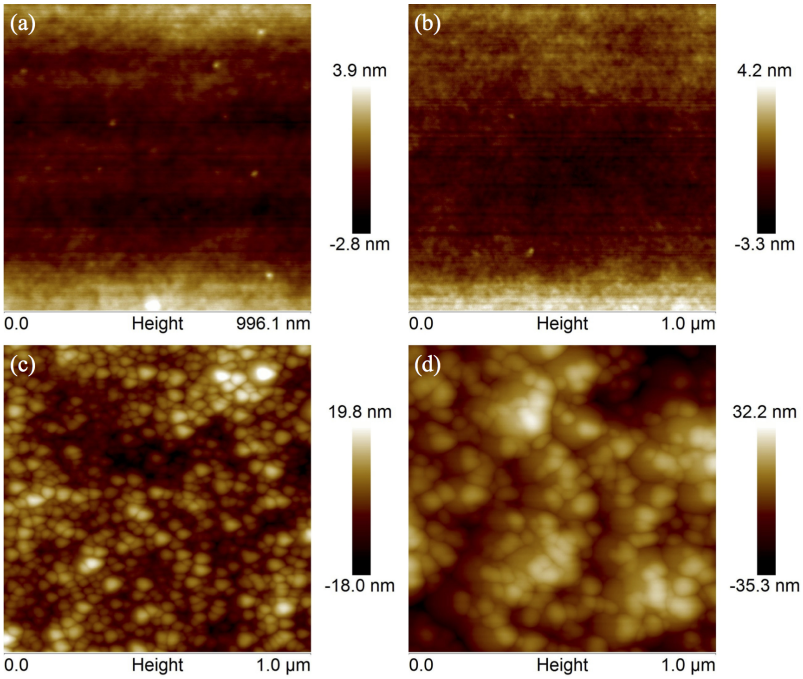

Figure 4.10: Surface characterization with AFM of planar thermally oxidizied copper oxide. The (a) 1-minute oxide and (b) 5-minute oxide develop a clearly seen oxide layer, but very small changes in surface roughness. The (c) 15-minute oxide demonstrates the development of larger grains. All of (a-c) were oxidized within a covered container, while (d) the 5-minute oxide was oxidized in completely open air.

The images show a trend of increasing roughness with longer oxidation time. In comparison with Castle's data, which are shown in parentheses in Table 4.1, it is clear that a more controlled environment has a large impact on the development of the oxide layer. For shorter-duration oxidation, the roughness values are fairly close - within 0.5 nm for the 1- and 5-minute samples. However, as the oxidation time increases to 15 minutes, the roughness drastically surpasses values measured by Castle [4]. This effect is also seen on the spheres in which samples that were oxidized in open air exhibit a much higher upper voltage limit than any other copper oxide spheres. These values are shown and compared in Table 4.1.

Table 4.1: Values related to the roughness of the thermally oxidized copper oxide. The roughness of copper oxide in this research seems to increase from 1 to 15 minutes whereas the values of roughness do not develop a trend in Castle's data before 15 minutes elapses. Castle's data are shown in paretheses.

Value	1 min (Castle 45 sec)	5 minute	15 minute
Z range (nm)	8.01 (23)	6.71 (9.7)	40.2 (10.2)
SA Difference (%)	0.174 (2.98)	0.630 (2.59)	6.84 (2.76)
Rq (nm)	1.14 (1.62)	1.18 (0.953)	5.22 (1.01)
Ra (nm)	0.917 (1.08)	0.956 (0.753)	4.1 (0.799)
Rmax (nm)	7.94 (23)	6.52 (9.7)	40.2 (10.2)

The values in Table 4.1 are used to compare to data gathered by Castle. The variables Z_{range} and R_{max} distance between the highest and lowest points. The value SA Difference is the difference between the 2-dimensional surface area and 3-dimensional surface area as a percentage. R_q and R_a are the RMS roughness and arithmetic average roughness, respectively.

4.3.4 Discussion On Etching and Oxidation Results

The results of the acetic-etched spheres were analyzed first and drove the need to conduct further etching/oxidation experiments. After oxidation of the acetic-etched spheres, it was clear by their electrical behavior that the oxide layer was not grown adequately. The I-V curves still demonstrated near-resistive behavior, but also hinted at highly insulated characteristics at lower voltages.

These data demonstrated that the acetic acid etch may have formed a cupric acetate layer on the surface of the spheres, preventing the successful growth of an oxide. The resulting surface of the spheres is depicted in Figure 4.11. With the development of a solid layer of cupric acetate on the external surface of the spheres, the oxidation process is inhibited at the temperatures that were used. Cupric acetate has a melting temperature of 115°C and a boiling temperature of 240°C. The oxidation processes being run at 100°C were not hot enough to affect the external cupric acetate layer, and thus could not oxidize the spheres.

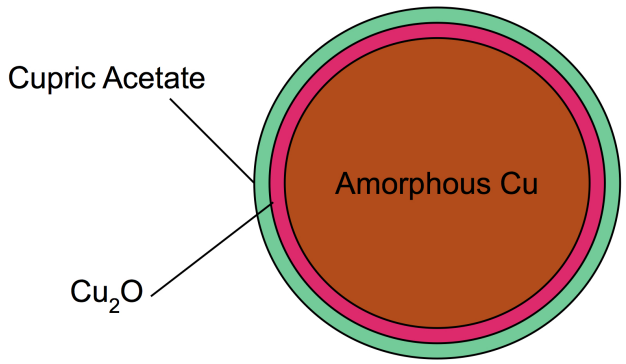

Figure 4.11: A copper sphere with a surface trapped by an cupric acetate layer. The use of acetic acid as an etchant resulted in the development of a cupric acetate layer, which prevented further oxidation on the spheres surface at the temperature being used.

For this reason, an inorganic etch was preferred to prevent further problems caused by organic chemical reactions. Nitric acid was selected for being the simplest inorganic acid available. The results of this etch demonstrated much better possibilities for developing an oxidized system as the spheres appeared slightly darker than the spheres etched with acetic acid after drying (shown previously in Figure 4.4), indicating a slight native oxide on the surface.

The hot-plate oxidation process was originally used as a secondary option. This process, however, resulted in an oxide with more repeatable electrical results. Consequently, the nitric-etched, hot-plate oxide spheres were used as the main experimental subjects. Current-voltage characteristics can be directly compared in the Appendix with Figure A.2 and Figure A.3.

4.4 Electrical Characterization and Memristive Behavior

While electrical characterization occurred throughout the development of different oxide systems, the nitric-etched, hot plate-oxidized spheres were primarily used for electrical characterization for the reasons discussed in Section 4.3.4. Among the tasks of characterization were defining basic rules such as the upper voltage limits of sphere systems and how increasing the number of spheres affects the electrical behavior, observing the memristive behavior of cuprous oxide on a spherical system, observing and defining the primary conduction mechanisms of the spheres, and characterizing the pressure-activated conduction and memristive characteristics.

4.4.1 Defining Basic Circuit Behavior and Voltage Limitations

Among the first tests conducted on the cuprous oxide spheres was to confirm the series characteristics of the spheres when placed in a 1-dimensional chain. This test was done by measuring the upper voltage limit on sphere chains of increasing length. For this examination, as-received spheres that had not been etched were oxidized on a hot plate for 5 minutes and used for electrical measurements. Figure 4.12 shows that the voltage limit

increased linearly with the number of spheres, indicating the behavior of a series circuit system. These results were used to infer the series behavior of all other sphere systems. Additionally, defining upper voltage limits was very useful for conducting primary I-V traces to ensure that measurements could be done without over-biasing a particular set of

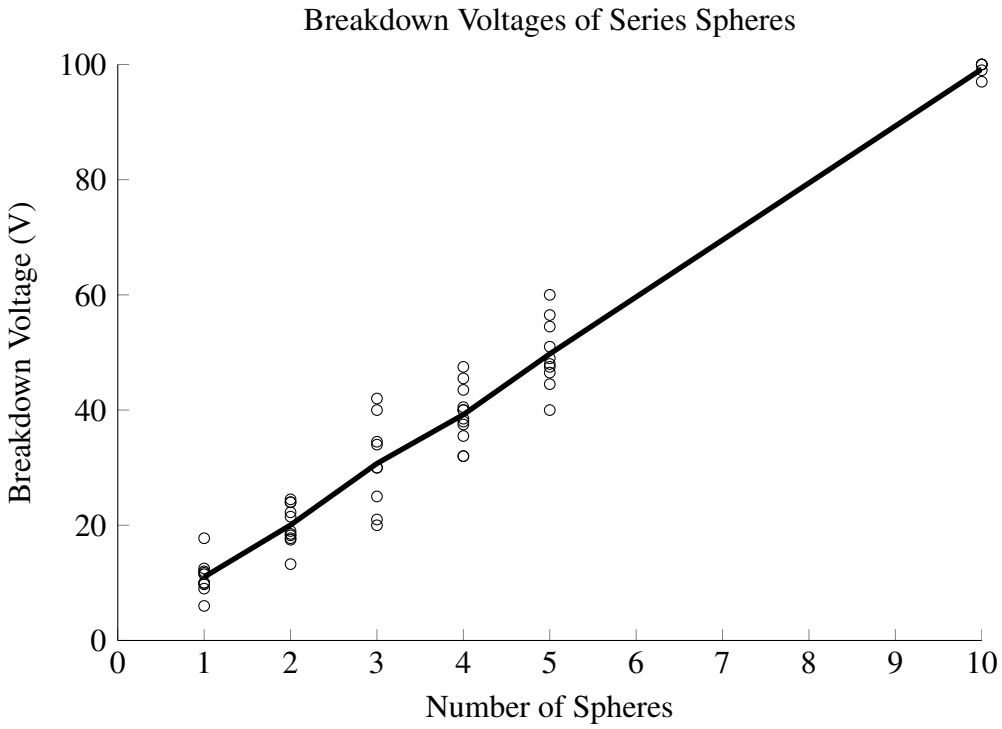

Figure 4.12: The upper voltage limits of a chain of spheres increases linearly. This set of data captured the upper voltage limits of spheres that were oxidized for 5 minutes without having been etched.

spheres. Accordingly, the upper voltage limit of each system was measured and averaged. Table 4.2 lists the results of these voltage limits for each sphere system.

4.4.2 Pressure-activated Memristive Characteristics

Using the voltage limits as a guide, I-V traces were conducted to characterize the 1-dimensional sphere chains for various oxide systems. The results here reveal the

Table 4.2: Summary of upper voltage limits per sphere for each type of sphere that was electrically characterized. For each sphere system, ten current-voltage measurements were taken. As the oxidation time increases, the voltage limit increases.

Oxide Sphere Type	Average Breakdown Voltage (V)	Standard Deviation
1 min, HP	2.87	1.86
5 min, HP	4.53	1.10
15 min, HP	6.90	0.57
5 min, No Etch	9.95	1.19

characteristics of the nitric acid-etched spheres that were oxidized on a hot-plate system. These results demonstrate sphere chains made up of five spheres for each oxide system. To demonstrate the stable condition of the oxides and their ability to withstand the voltage traces without experiencing any further electroforming, the sphere systems were repeatedly measured with I-V curves prior to being tested with various compressive applied forces. The current-voltage data was then integrated using a summation method to show the steadiness of the hysteresis, or the area on the plot that the curves enclose. These curves are shown in Figure 4.13.

These data indicate that for sphere systems that were oxidized for longer periods of time, the I-V curve exhibits less hyseteresis. After demonstrating the stability of the oxides for each sphere, compressive tests were conducted. Figure 4.14 shows the change in current-voltage characteristics of each sphere system at each level of compressive applied force.

As this plot shows, the maximum current for each I-V sweep increases as the sphere chains are compressed. The intervals of applied force translate to compressive displacements on the scale of 10 μm. It is clear in this data that an increasing oxide thickness results in lower maximum current and greater resilience. In this thesis, the

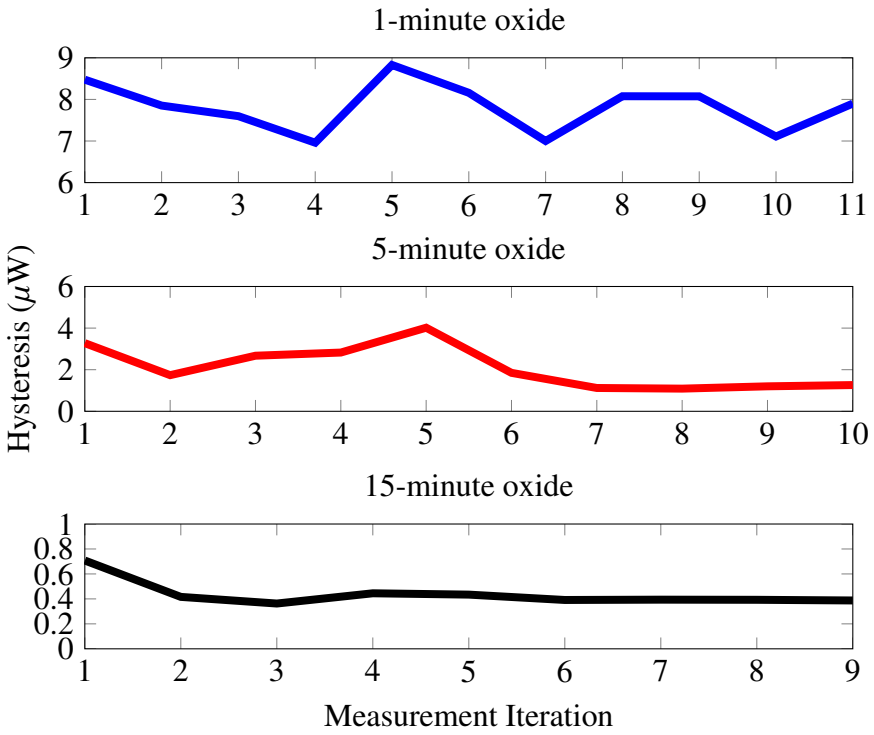

Figure 4.13: The I-V curves for 1-, 5-, and 15-minute oxides were measured 10 times each. These data were gathered to demonstrate the repeatability of the measurements and the stability of the oxide prior to taking I-V measurements with various applied forces.

resilience will be used to describe the amount of force the spheres can be subjected to before reaching dielectric breakdown during an I-V trace. This data is important because it shows the entire electrical response of the copper spheres during compression; however, the data can be summarized by plotting the hysteresis in μW. The summarized memristive response is plotted in Figure 4.15.

As Figure 4.15 indicates, each oxide thickness exhibits hysteresis that increases in an approximately linear trend during compression. As indicated by the data, the 1-minute oxide could only sustain about 12 mN of compression while the 5- and 15-minute oxides were measured for a full spectrum of compression and decompression from 0 to 22.3 mN. The resilience of the 5- and 15-minute oxides prompted a further observation about the

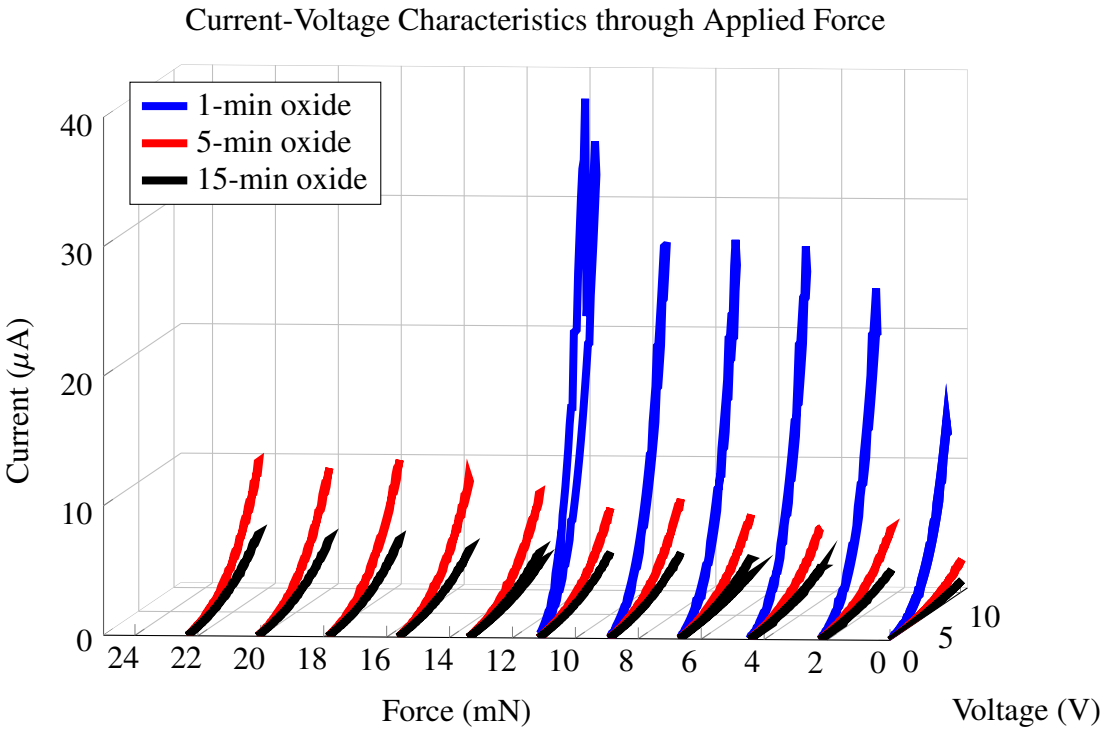

Figure 4.14: The I-V traces of 1-, 5-, and 15-minute oxide sphere systems over compression intervals of about 2.5 mN. The data indicates that increasing the oxide thickness results in lower sensitivity and greater resilience. The 1-minute oxide shows he greatest sensitivity to compressive forces, but reaches dielectric breakdown after just 12 mN of compressive force.

electrical characteristics during compression and decompression. These compressive and decompressive changes can be seen in Figure 4.16 and Figure 4.17. As the spheres are compressed, the current tends to reach higher values. As they are decompressed, the current values decrease, but not to the same magnitude.

For the 15-minute oxide spheres, current-voltage measurements were able to continue while decompressing beyond the original point where electrical contact was first established. This contrasts with the 5-minute oxide spheres because the spheres fell out of electrical contact upon decompressing to the original position. This behavior indicates that perhaps high temperatures caused by Joule-heating are causing copper metal to melt

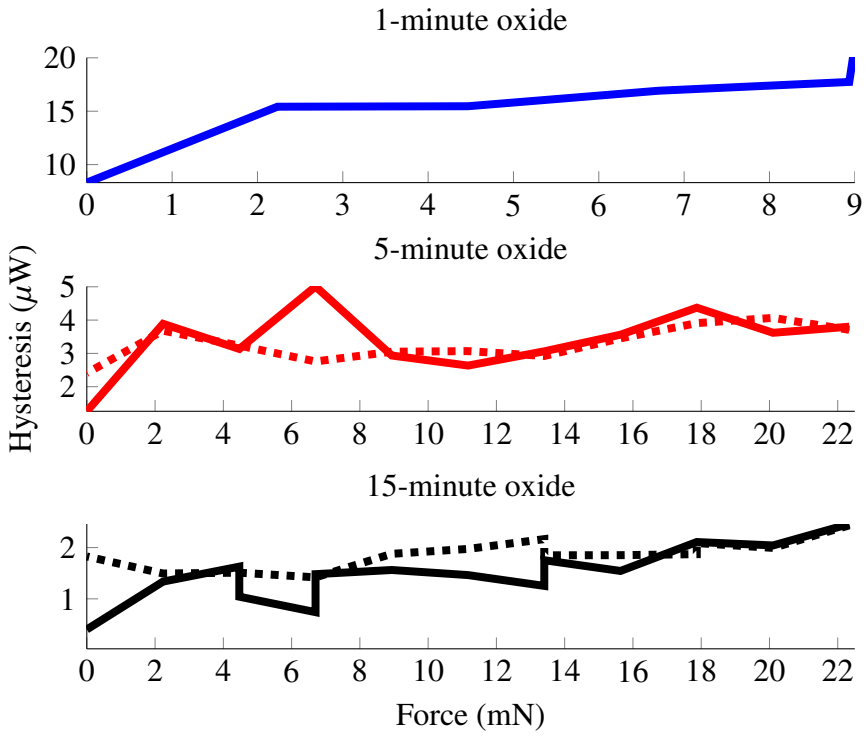

Figure 4.15: The hysteresis of the I-V curves plotted against compressional force. These data summarize the memristive sensitivity for each oxide thickness in the copper spheres and indicate the hysteresis increases linearly as spheres are compressed. For the 5- and 15-minute oxide spheres, the dashed lines indicate the hysteresis during decompression.

and induce sticking between spheres. However, this would suggest that Joule-heating is causing temperatures to reach up to about 1360 K. Otherwise, it may indicate that with a thicker oxide layer, establishing an electrical contact required more force.

The effect of oxide thickness on sensitivity and resiliency indicates an important design trade-off. However, this trade-off of sensitivity vs. resiliency exists within a certain range of oxide thicknesses. The upper limit of oxide thickness is established with the need for a thin-enough oxide to allow for memristive behaviors to take place. A lower limit of oxide thickness is set by oxidation capability. As these data indicate, the memristive behavior is quite inferior to previously documented copper oxide memristors [10]. However, memristive behavior is still clearly present and is investigated.

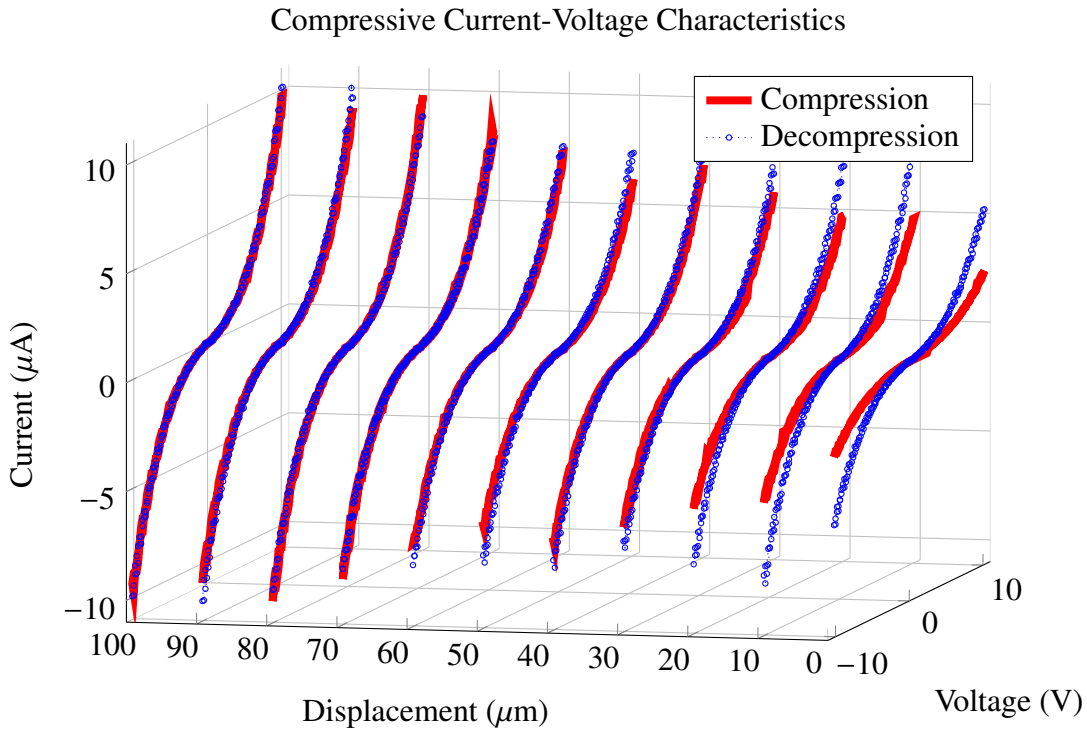

Figure 4.16: The I-V characteristics of 5-minute oxide spheres under compression and decompression. During decompression, the I-V curves can be seen to follow very closely with those during compression until lower levels of compression are reached.

4.4.3 Memristive behavior

The novel characteristic of the spheres systems is the memristive behavior of cuprous oxide. Cuprous oxide has been shown to have memristive characteristics [4]. To demonstrate these results, single plots are used to point out the hysteresis loops that occur in the I-V curves. Figure 4.18 shows the hysteresis loops of the 1-minute oxide copper sphere system.

As shown here, the I-V sweep results in tight hysteresis loops. Memristive switching can be quantified by calculating an ON-OFF ratio (the ratio of resistances in the on and off state) or by calculating the area of the hysteresis loop in units of Watts. Whereas many copper oxide systems have been shown to have more significant memristive behavior with

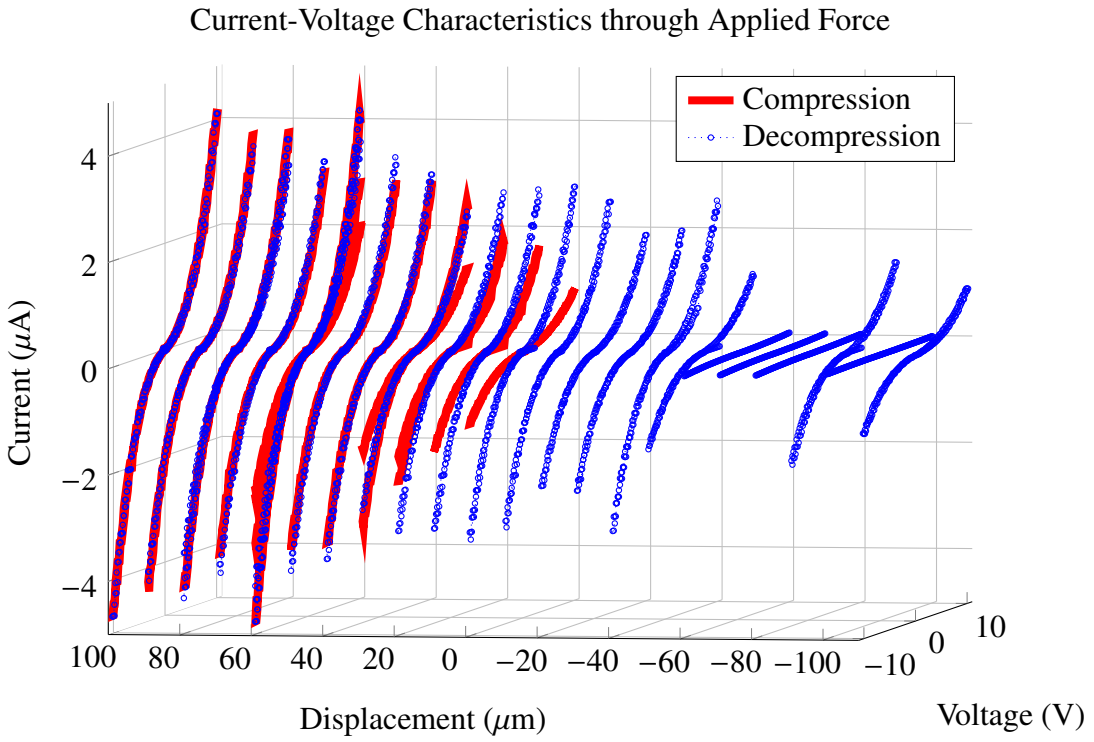

Figure 4.17: The I-V characteristics of 15-minute oxide spheres under compression and decompression. These spheres followed a similar pattern as the 5-minute oxide spheres and were shown to still operate beyond the original compression point in which electrical contact is first established. This decompression continued for up to 100 μm.

ON-OFF ratios ranging from 80 to over 3000, our systems appear to have an ON-OFF ratio that maxes out at about 3 [10, 23]. While the memristive characteristics are weaker, these results demonstrate promise for future research.

It is believed that the main dissimilarity between this copper oxide system and other recorded copper oxide systems is the electrode material [53]. This system is effectively a series of symetric Cu/Cu_2O/Cu devices, as the diagram in Figure 1.1 shows. It is repeated here for convenience.

As pointed out by Yang, the electrode material can play an important role in the memristive behavior of copper oxide devices, with one of the main parameters being the

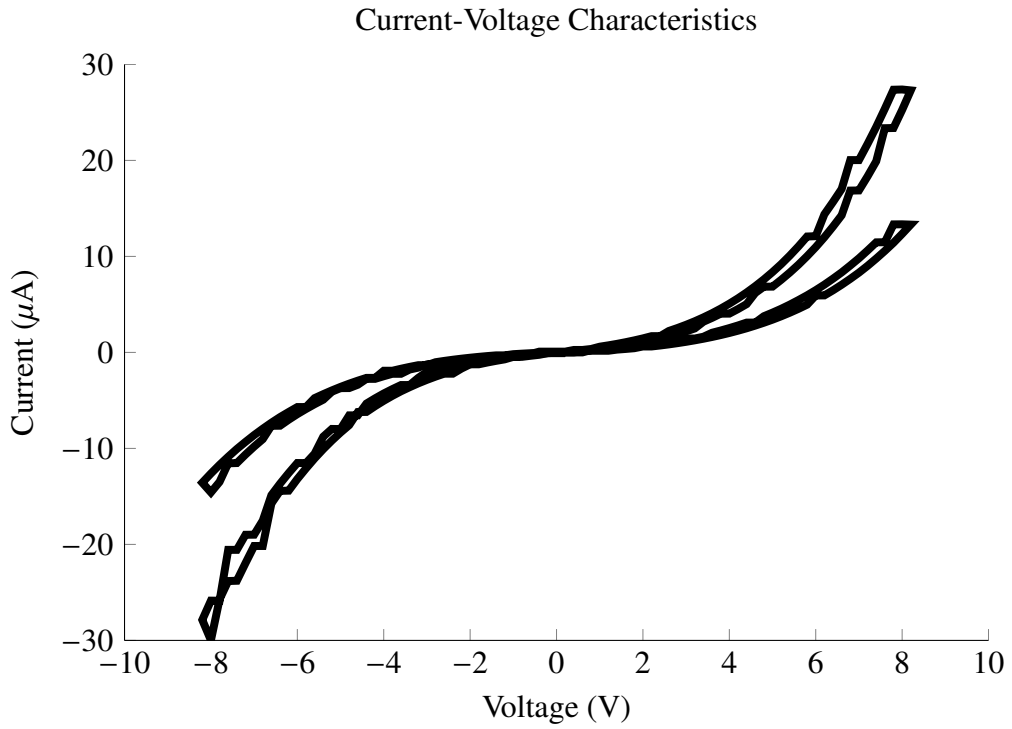

Figure 4.18: Hyseteresis loops demonstrating the memristive behavior of the copper spheres. This plot shows two I-V curves for the 1-minute oxide. The higher-current curve is during compression while the lower-current curve is not during compression.

work function [53]. It was shown that when using an electrode with a work function less than the work function of copper oxide, the memristive behavior is weaker. Cuprous oxide has a work function of about 4.84 eV while the work function of copper is about 4.35 eV [53]. Since copper oxide is a p-type semiconductor, the work functions indicate that there are schottky barriers on both ends of the copper oxide interface. The lack of an ohmic contact may be preventing increased memristive behavior. The work function of platinum, for example, is about 5.1 and provides much more significant hysteresis loops in the literature. This problem however may be due to the work function at just one end of the device, meaning that the symmetrical schottky contacts may be the cause for the lack of resistance switching. It has been suggested that resistance switching requires asymmetric

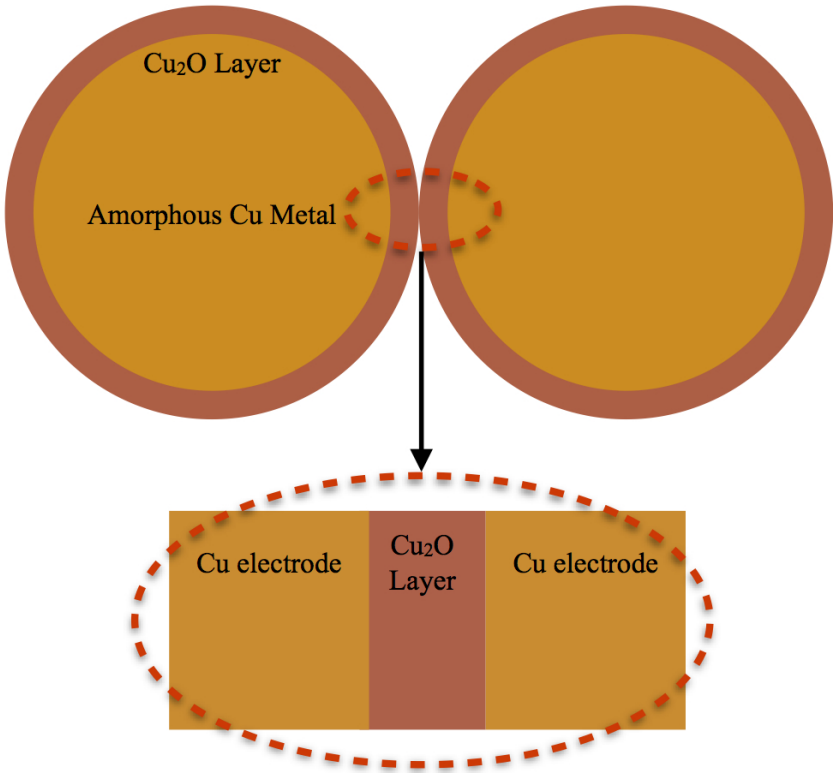

Figure 4.19: The electrode interfaces of the sphere chain system. There are essentially a series of Cu/Cu_2O/Cu devices in which the work functions of Cu and Cu_2O are 4.6 and 4.84, respectively.

devices having an ohmic contact at one electrode and a non-ohmic contact at the other electrode [51].

An important factor for these metals is their mechanical properties. Since this system involves the use of compressive forces, it is important that the materials can withstand the applied force without being easily damaged. Specifically, the Young's modulus is a good indicator of the stiffness of a material. Platinum has a Young's modulus of 168 GPa, comparable to that of copper's 117 GPa.

Another difference between this copper oxide system and other recorded copper oxide systems is the specific oxide in use. This research has used a stable thermally grown cuprous oxide layer. Other research, however, has shown strong memristive behaviors

using aluminum, molybdenum, and platinum electrodes on Cu_xO device [10, 23, 25]. It is possible that using the less-stable Cu_xO material provides a greater number of oxygen vacancies. This greater availability of oxygen vacancies may help in the formation and dissociation of a conducting filament.

4.4.4 Conduction Mechanisms

Despite the weaker memristive behavior, the cuprous oxide sphere system demonstrates a measurable conduction mechanism. As the I-V curves in Figure 4.18 show, the main electrical characteristic is a non-linear relationship between current and voltage. Dong and Yang among others have attributed the behavior of this type to a conduction mechanism relating to the Mott-Gurney law [10, 17]. The current-voltage relationship that results from the Mott-Gurney law can be expressed as

$$J = \frac{9}{8}\frac{\epsilon_r \epsilon_0 \mu V^2}{d^3}. \tag{4.1}$$

In Equation (4.1), ϵ_r and ϵ_0 are the dieletric constant and permittivity in free space, μ is the mobility of the majority charge carrier, d is the thickness of the insulating material, and V is the applied bias. Indeed, these curves appear quadratic in nature, however curve-fitting the data reveals other potential conduction mechanism for this system. Specifically, an exponential square root similar to that of the field-enhanced thermionic emission mechanism appears to be a potential answer. The equation for the field-enhanced thermionic emission is described by

$$J = \frac{4\pi q m_h k^2}{h^3} T^2 e^{\frac{-(\phi_B - \alpha\sqrt{\frac{V}{d}})}{kT}} \tag{4.2}$$

in which q is the electron charge, m^* is the effective mass of the majority charge carrier, k is the Boltzmann constant, h is Planck's constant, T is the temperature, ϕ_B is the barrier potential, α is the Schottky coefficient ($3.79 * 10^{-5} \frac{\mathrm{eV}}{\sqrt{\mathrm{V/m}}}$), d is the thickness of the

insulating material, and V is the applied bias. Figure 4.20 shows some curve fits for a 0 to 8 V I-V sweep of the 1-minute oxide.

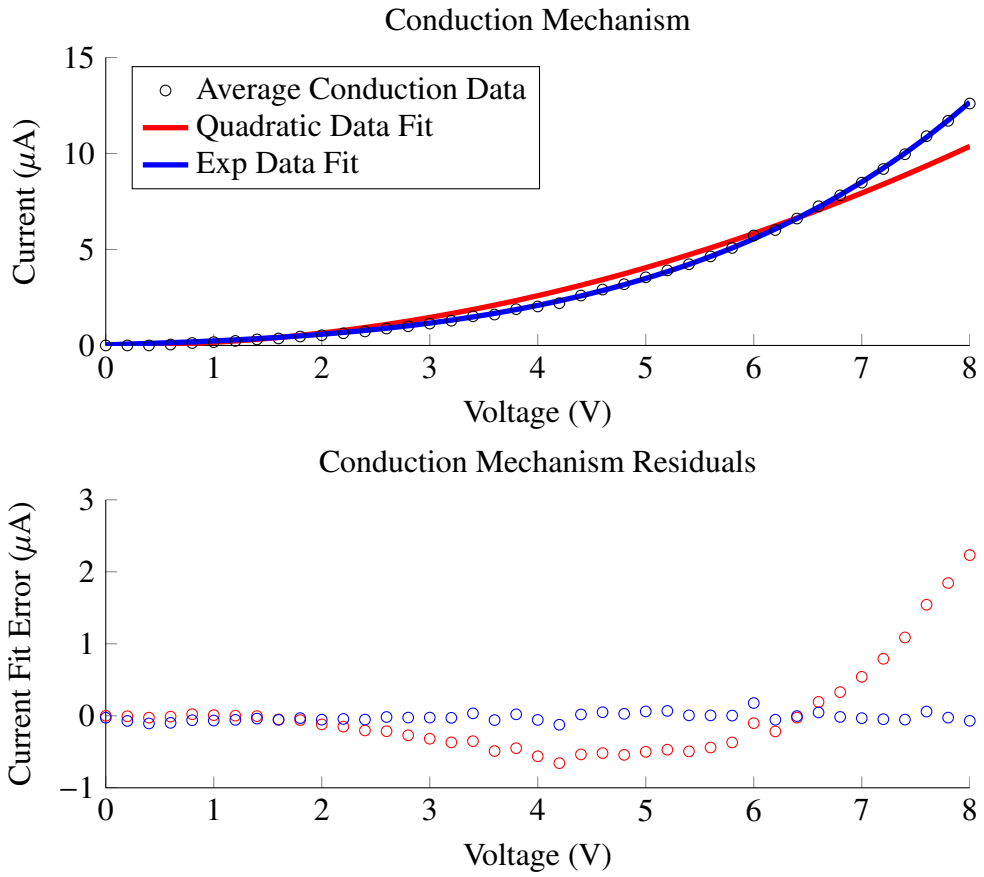

Figure 4.20: Curve fitting functions for I-V data acquired on the 1-minute oxide sphere system. Curve fitting functions were based on the proportionality between current and voltage that is described by conduction equations.

These curve fits were chosen based on the equations of potential conduction mechanism. As the data points out, one of the best fits is the exponential fit. This data has a correlation (r^2 value) of 0.999 and, as Figure 4.20 shows, it results in smaller residual values than a quadratic relationship. As these equations indicate, there are several constants that are dependent on the material and geometry. The nature of this research, however, makes the precise acquisition of these constants difficult. As a solution,

information has been gathered from literature on cuprous oxide. These constants can be found in Table 4.3.

Table 4.3: These constants were used to plot the equations used that describe various conduction mechanisms. Many of these values are reported from various research and have been adjusted within the limits of what has been found in other research [14, 20, 26, 29, 31, 43].

Symbol	Parameter	Value
α	Schottkey Coefficient	$3.79 * 10^{-5}$ $\frac{\text{eV}}{\sqrt{\text{V/m}}}$
ϵ_r	Dielectric constant	7.11
μ	Carrier Mobility (holes)	0.08 - 100 $\frac{\text{cm}^2}{\text{Vs}}$
m_h	Effective hole mass	0.58
ϕ_B	Barrier Potential	0.66 eV

These constants were gathered from various sources and in some cases slightly adjusted within the limits of reported values. For instance, the electron activation energy, E_{ae} has been reported to be between 0.16 and 0.42 eV and as high as 0.68 eV [20, 26, 31]. Likewise, the hole mobility μ_h has shown to be even more elusive as it strongly depends on oxidation conditions [29]. Values for thermally oxidized cuprous oxide have been reported to be as low as 0.08 $\frac{\text{cm}^2}{\text{Vs}}$ when oxidized at 300K and as high as 70-100 $\frac{\text{cm}^2}{\text{Vs}}$ when oxidized in temperatures up to 1070 K [14, 26, 43]. Other constants such as the density of states in the valence band and the barrier potential were calculated using textbook values. These values were used within the equations listed above for various conduction mechanisms and plotted against the same voltages used in I-V measurements.

Figure 4.21 indicates that using values that are common in other research for cuprous oxide, these equations can be plotted comparatively to the experimental data gathered from this research. For these plots, estimations based on findings in other literature were

made on the values of the temperature, conductive filament width, oxide thickness, and effective hole mass in order to calculate the parameters for hole mobility and barrier potential from the resulting best-fit curve. The estimations that were used for conduction filament width affect the current for a given current density. Ranges for conductive filament radius have been recorded between 5 to 100 nm [35, 54]. This calculation simply took a middle estimate of 50 nm. In simulations, temperatures have been calculated to reach up to about 800 K [17, 35]. As noted in Table 4.3, the effective hole mass used for these calculations is 0.58 m_e. Finally, as noted in Chapter 3, the oxide thickness for the 1-minute oxide is estimated to be about 3.72 nm. The outcomes of these curve fits can be cross-examined to the ranges for mobility and barrier potential that are provided in the literature.

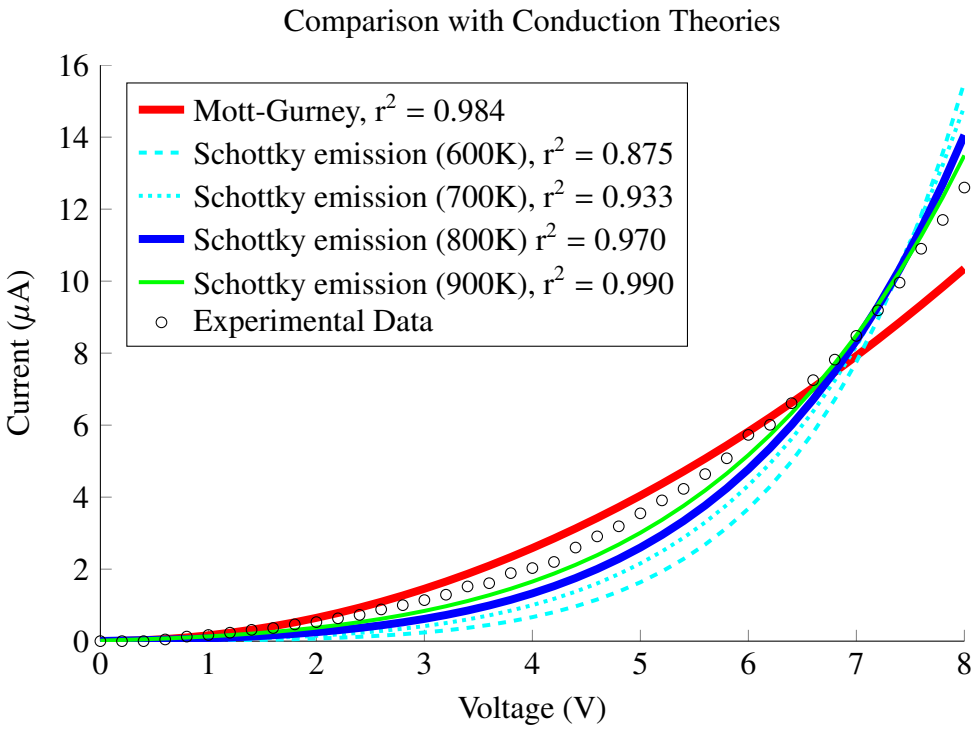

Figure 4.21: Experimental data plotted with equations describing conduction mechanisms. It can be seen that the Mott-Gurney law follows closely to the experimental data. Additionally, the Schottky emission mechanisms are plotted in a summation.

These plots help provide a working insight to the possible conduction mechanisms that dominate in the cuprous oxide memristive spheres. In the curve fit based on the Mott-Gurney law (Equation (4.1)), the hole mobilty is calculated to be 0.15 $\frac{cm^2}{Vs}$, which falls well into the range listed in Table 4.3. In the curve fit based on field-enhanced thermionic emission, the barrier potential is calculated to be 0.936 eV, which is not unreasonable for a barrier potential value. Using Equation (4.2), the slight reduction in temperature results in a lower calculated barrier function. Curves fitted for 600, 700, and 900 K are also plotted to demonstrate variation in barrier potential as the estimation for temperature is adjusted. These curve fits suggest that as the curves are fitted for a higher estimated temperature, the corresponding barrier potential is higher and the resulting r^2 value is better, indicating a better fit.

4.5 Summary

The copper spheres have been characterized for their surface characteristics as well as their electrical behavior. It was shown that the copper spheres maintained a stable memristive state within a specific voltage range for each oxide type. The spheres were then compressed while characterized for their I-V behavior. These data indicated that the 1-minute oxide is frigile compared to the 5- and 15-minute oxides. It was shown that for the 15-minute oxide, the spheres were able to decompress beyond the starting point by 100 μm. The memristive behavior of the spheres was characterized and discussed. It is suggested that material selection for the force probe may play a role in the success of the memristive behavior. Additionally, the conduction mechnanism was characterized. The conduction data indicated that the Mott-Gurney and field-enhanced thermionic emission mechanisms were potential mechanisms by which the copper oxide on the spheres conducts a current.

V. Conclusions

5.1 Overview

This chapter reviews the main points of this research, provides a conclusion on the findings, and provides suggestions for future research. The main aspects of this research were characterizing the conduction mechansims, memristive behaviors, and system protection capabilities of copper oxide spheres.

5.2 Conclusion

Characterizing and testing 1-dimensional chains of memristive copper oxide spheres demonstrated the feasibility and further research potential of their use as a system protection technology. The application of a thin oxide surface on each sphere provide a practical starting place for researching memristive behaviors in transition metal oxides on copper microspheres. Placing these spheres in contact with one another and applying a bias can detect changes in electrical behavior under applied force. The primary attributes of this research are fundamental to two particular topics: the memristive characterization of the metal oxide material of the spheres and the characterization of the spheres as an system protection technology.

5.2.1 Memristive characteristics

While the data suggest a slight degree of resistive switching that occurs during a voltage sweep, it is clear that these memristive behaviors are not as significant as noted in most other resistive switching research. Visual inspection of the I-V curves alone indicates that the hysteresis loops in this research are very tight compared to those seen in past work using copper oxide [4, 10]. Nonetheless, the memristive behaviors of the copper oxide spheres were shown to be stable over several measurements, as indicated in Figure 4.13. By measuring the hysteresis as the area of the loop in μW, the data indicated that the 1-,5-,

and 15-minute oxide spheres each exhibited repeatable memristive behavior in which the hysteresis was calculated to about 8, 2, and 0.5 μW, respectively.

5.2.2 Characterization as an system protection technology

The primary data of this research has shown that the cuprous oxide microspheres can detect physical interferences of compressional applied force for as low as about 2.5 mN. As Figure 4.15 shows, a thicker oxide on the sphere results in a lesser response in the change of hysteresis. However, thicker oxides also demonstrated a greater level of force before experiencing dielectric breakdown. The comparison of data between differing oxide thicknesses indicates a design trade off between sensitivity and resilience.

The overall behavior of the spheres in a 1-dimensional chain indicate different possible methods of use as a system protection technology:

1. Briefly running current-voltage measurements every few minutes and monitoring changes that occur between samples
2. Constantly holding a low voltage and monitoring changes in current when an interference is detected
3. Holding the spheres at a low voltage at a force large enough such that any physical interference will cause a complete dielectric breakdown, providing a large current spike

In any of these controlled system protection applications of the cuprous oxide spheres, it is possible to perform basic interference monitoring. This research has shown that the devices have been characterized such that testing and characterization can begin on the 2-dimensional configuration.

5.3 Future Research and Recommendations

5.3.1 Materials Research

The performance of the cuprous oxide on a copper sphere as a memristive device prompted further literature research on copper oxide devices. Copper oxide has a strong prospect as a memristive material and likewise, the system protection capability of a

system of memristive copper oxide spheres has been demonstrated. However, there are several possible methods of improving the system as a whole. One of the problems faced with creating a memristive interface is the selection of materials. It has been shown that certain materials provide resistance switching characteristics that are much more significant than others. Yang showed that simply changing the top electrode material can play a major role in the resistance switching capability of the entire device [53]. Similarly, it is well documented that the material of the insulator contributes to the overall device characteristic on the spectrum of thermal- and field-dominated memristive behavior [52]. Devices can be engineered to provide specific resistance switching results based on material properties such as the work function or resistivity. Copper oxide has been shown to have a strong memristive response in various literature with the switching mechanism varying from tri-stable switching, to either bipolar or nonpolar switching. It would worth researching the aspect of nonpolar switching as well as bipolar switching for the system protection purposes addressed in this research. Another possible option is the use of other materials. Titanium oxide has been a popular material in memristor research and may serve as a superior replacement to copper oxide as the insulator material in a memristive interface.

5.3.2 Oxide Surfacing

A major challenge in the characterization of the cuprous oxide spheres is the method of fabrication. Starting from an amorphous ball of copper, the spheres are cleaned with acid and thermally oxidized. For this research, acetic acid and nitric acid were used to clean the copper spheres in preparation for thermal oxidation. The nitric acid provided a smoothed surface and allowed for a reliable oxide to grow afterwards while the acetic acid seemed to have hinder the oxidation process at our chosen temperatures. While nitric acid has provided good results for surface preparation, there are several acids that may yet

provide better results. A handful of acids have been listed as etchants for cuprous oxide as well as several other metal-based materials [42].

The method of thermal oxidation in this research was relatively uncontrolled. Overall, it has been suggested that thermal oxidation can be inferior to other methods of applying an oxide layer such as plasma-enhanced atomic layer deposition or reactive DC magnetron sputtering [19, 56]. The process of thermal oxidation, however has been thoroughly investigated [24]. For this research, especially, thermal oxidation was important for providing a way to ensure that the full surface of the spheres developed an oxide layer. The ability to ensure a full oxide upon a spherical surface came at the cost of providing a fully controllable environment. Using a more controllable oxidation method would provide a more reliable oxide layer. An oxidation method that would be favorable would be one such that achieving a Cu_2O/CuO bilayer or Cu_xO layer is possible while still providing high throughput.

5.3.3 Identification of Material and Electrical Properties

One of the difficulties of this research was the geometry of the memristive interfaces. The spherical shape of the material makes difficult some measurement techniques that are standard for devices made on a planar substrate. This research made use of developing a comparable oxide film on a planar substrate to compare the surface features using AFM. This method may be usable to measure other parameters of the copper oxide such as the oxide thickness and resistivity. Additionally, these data could be gathered to show changes in device parameters for varying oxidation temperatures for thermal oxidation methods. Such information could be cross-references with previously recorded data and used to provide a rigorous characterization for future prototypes.

5.3.4 Preparedness of 2-dimensional Research

The purpose of this research was to provide a foundation for testing and developing the 2-dimensional and 3-dimensional sphere systems. This research has developed a

method of fabricating a memristive spherical interface, characterized electrical limits, demonstrated memristive behavior, and shown how the memristive behavior can serve as a system protection sensor. Using this information, it would be possible to develop a two-dimensional implementation using the memristive/insulating sphere pair as shown in Figure 5.1.

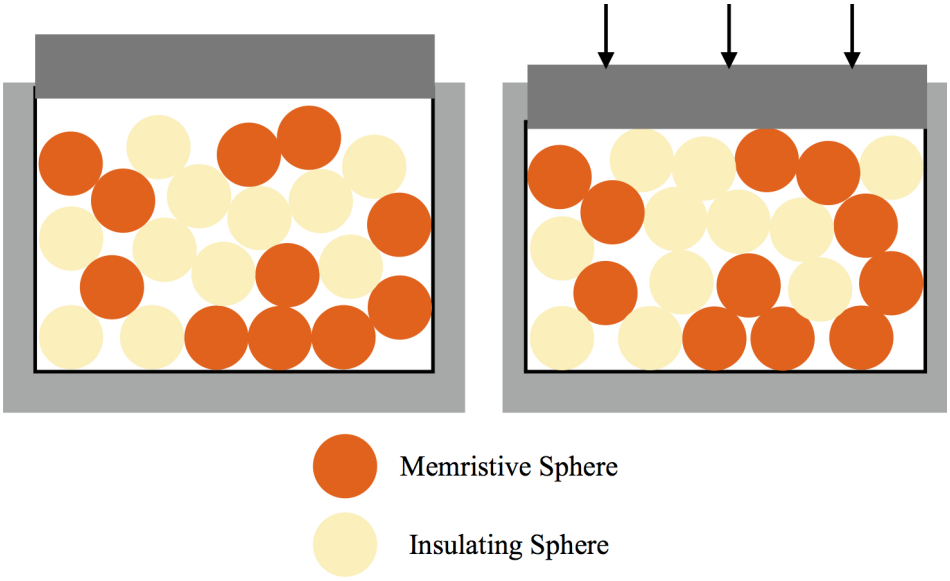

Figure 5.1: A demonstration of how the 2D implementation could be designed. Using a thick planar insulating material, the spheres can be randomly loaded into a lower level surface and covered by a glass shield to contain the spheres in two-dimensions. One side of the containment area can be movable to allow of measured compression of the 2D system of spheres.

Fundamentally, this research has provided the tools that are necessary to reach the next sequence of research needed to develop a working system protection technology.

Appendix A: Current-Voltage Characteristics

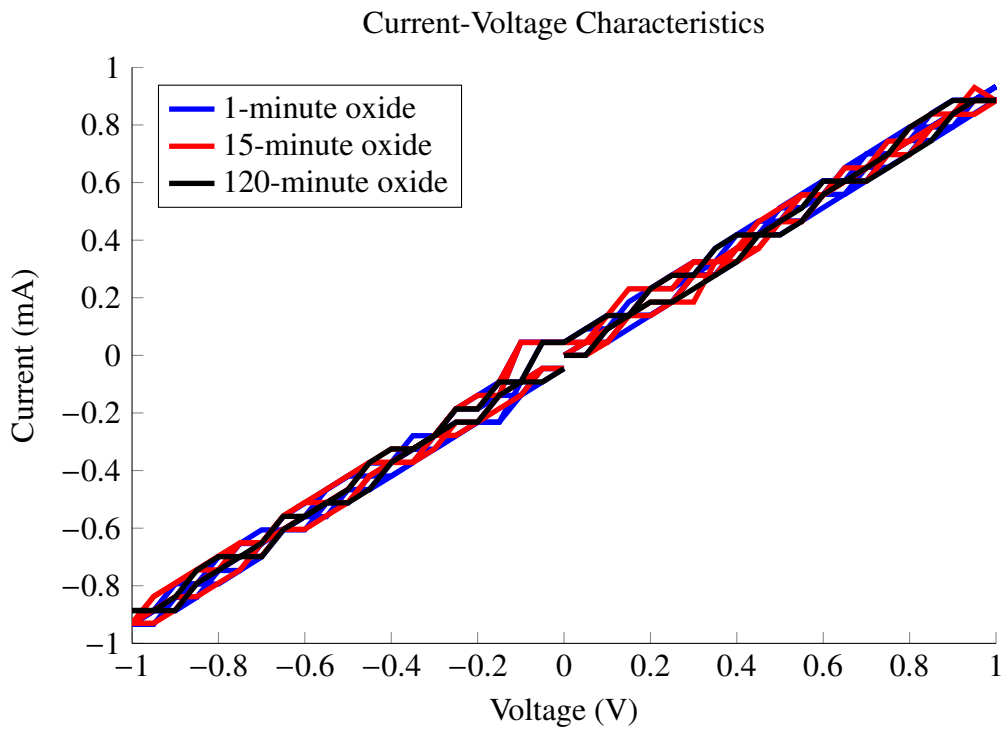

Figure A.1: Current-voltage characteristics for acetic acid-etched spheres oxidized in a quartz tube furnace for 1,15, and 120 minutes.

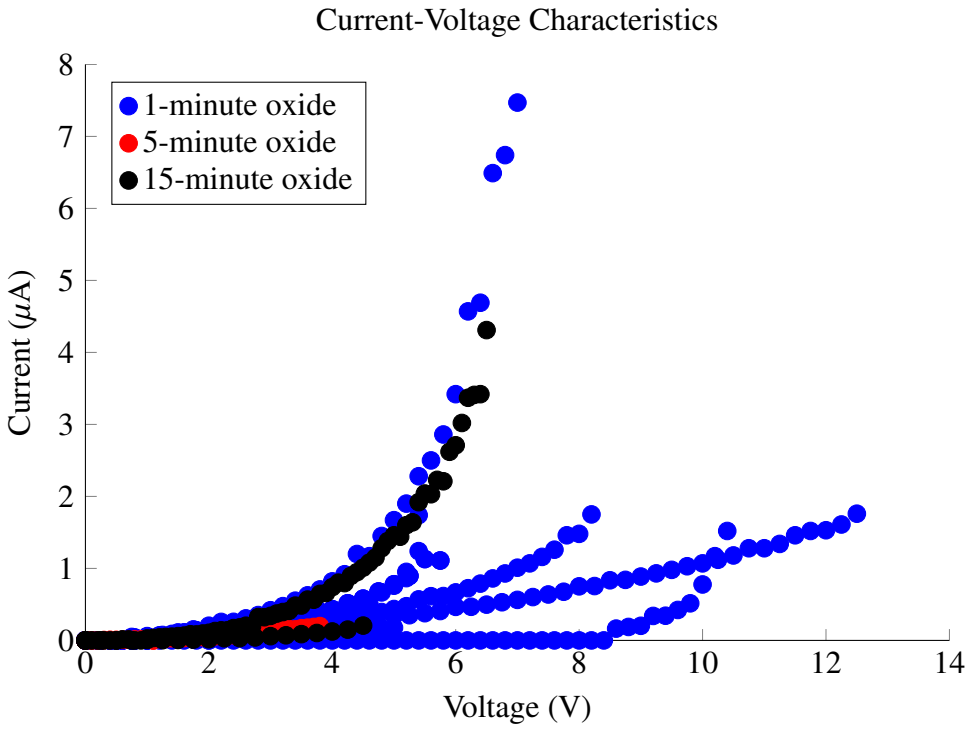

Figure A.2: Current-voltage characteristics for nitric acid-etched spheres oxidized in a quartz tube furnace for 1, 5, and 15 minutes. The inconsistent data for these spheres can be compared to those in Figure A.3 in which data appears more reliable and defined.

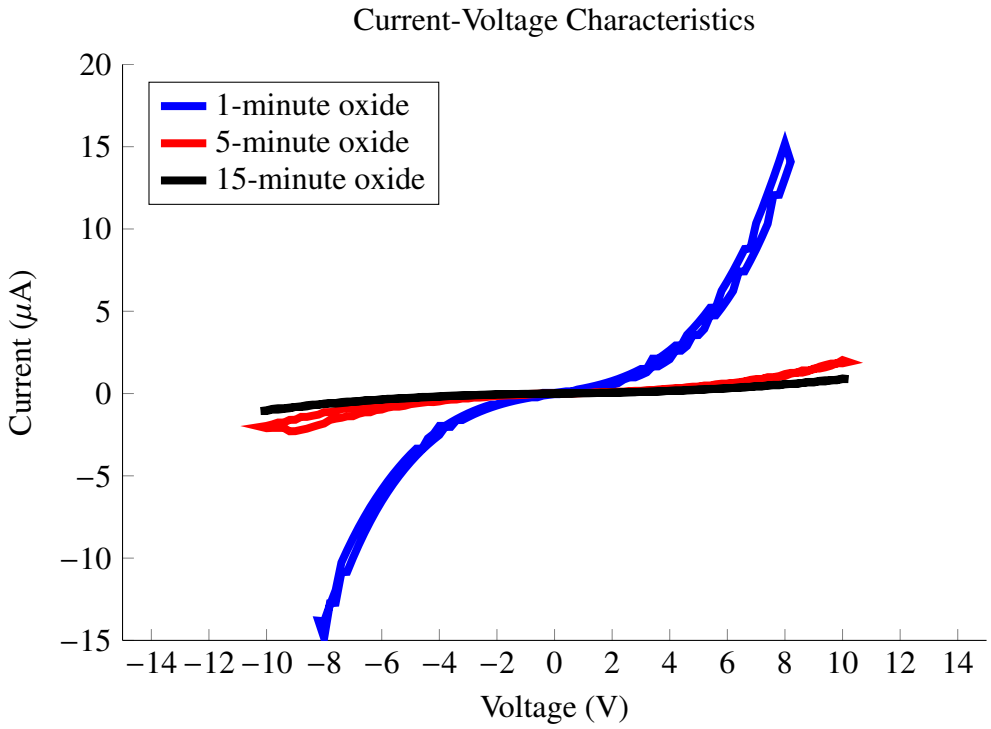

Figure A.3: Current-voltage characteristics for nitric acid-etched spheres oxidized in on a closed hot plate in atmosphere for 1, 5, and 15 minutes. Each sphere is traced about 10 times, showing how these sphere systems exhibit reproducible data.

Appendix B: Oxidation Rates

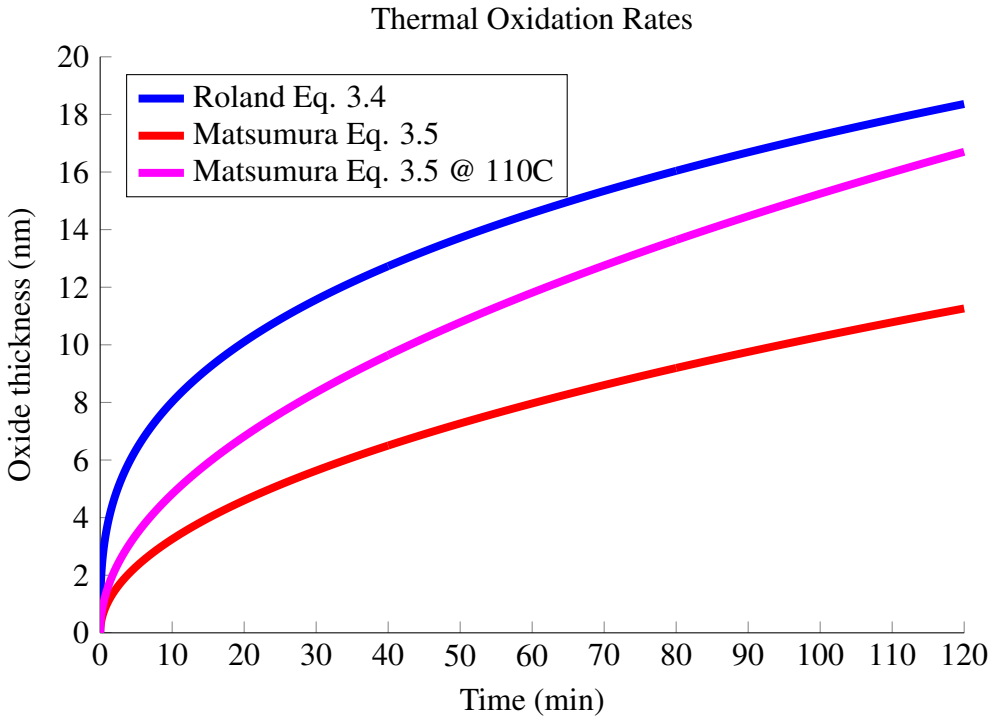

Figure B.1: Oxidation rates for copper at 100 °C by two different formulas. This plot shows how closely these formulas agree. These data are used to provide an estimate for oxide thicknesses.

References

[1] Anderson, Ross. *Security Engineering: A Guide to Building Dependable Distributed Systems*, second edition Chapter 13: Nuclear Command and Control. Wiley Publishing, Inc., Indianapolis, IN, 2008.

[2] Borghetti, Julien, D.B. Strukov, M.D. Pickett, J. Joshua Yang, Duncan R. Stewart, and R. Stanley Williams. "Electrical transport and thermometry of electroformed titanium dioxide memristive switches". *Journal of Applied Physics*, 106:124504–1 – 124504–5, Dec 2009.

[3] Campbell, W.E. and U.B. Thomas. "The Oxidation of Metals". *Journal of the Electrochemical Society*, 91, Issue 1:623–640, 1947.

[4] Castle, Brett. *Memristive Properties of Thin Film Cuprous Oxide*. Master's thesis, School of Engineering and Management, Air Force Institute of Technology, Wright-Patterson AFB OH, March 2011.

[5] Chavez, K.L. and D.W. Hess. "A Novel Method of Etching Copper Oxide Using Acetic Acid". *Journal of the Electrochemical Society*, 148, Issue 11:G640–G643, 2001.

[6] Chua, L. "Memristor - The Missing Circuit Element". *IEEE Transactions on Circuit Theory*, Ct-18, No. 5:117–123, Sept 1971.

[7] Chua, L. "Resistance switching memories are memristors". *Applied Physics A*, 102:765–783, Jan 2011.

[8] Dearnaley, G., A.M. Stoneham, , and D.V. Morgan. "Electrical phenomena in amorphous oxide films". *Rep. Prog. Phys.*, 33:1129–1191, 1970.

[9] Department of Defense. "Acquisition Systems Protection Program", March 1994.

[10] Dong, R., D.S. Lee, W.F. Xiang, S.J. Oh, D.-J. Seong, S.H. Heo, H.J. Choi, M.J. Kwon, S. N. Seo, M.B. Pyun, M. Hasan, and Hyunsang Hwang. "Reproducible hysteresis and resistive switching in metal-CuxO-metal heterostructures". *Applied Physics Letters*, 90:042107–1 – 042107–3, Jan 2007.

[11] Fujiwara, Kohei, Takumi Nemoto, Marcelo J. Rozenberg, Yoshinobu Nakamura, and Hidenori Takagi. "Resistance Switching and Formation of a Conductive Bridge in Metal/Bonary Oxide/Metal Structure for Memory Devices". *Japanese Journal of Applied Physics*, 47:6266–6271, 2008.

[12] Huber II, Arthur F. and Jennifer M. Scott. "The Role and Nature of Anti-Tamper Techniques in U.S. Defense Acquisition". *Acquisition Review Quarterly*, 335–368, Fall 1999.

[13] International Atomic Energy Agency. "The Physical Protection of Nuclear Material and Nuclear Facilities", June 1999.

[14] Jeong, S. *Thin zinc oxide and cuprous oxide films for photovoltaic applications*. Ph.D. thesis, University of Minnesota, Minnesota, 2010.

[15] Jiang, W., R. J. Kamaladasa, Y. M. Lu, A. Vicari, R. Berechman, P.A. Salvador, J. A. Bain, Y. N. Picard, and M. Skowronski. "Local heating-induced plastic deformation in resistive switching devices". *Journal of Applied Physics*, 110:054514–1 – 054514–6, Sept 2011.

[16] Keil, P., D. Lützenkirchen-Hecht, and R. Frahm. "Investigation of Room Temperature Oxidation of Cu in Air by Yoneda-XAFS". *Proceedings of the X-Ray Absorption Fine Structure 13th International Conference*. Stanford Synchrotron Radiation Laboratory, California, 2006.

[17] Kim, Sungho, Sae-Jin Kim, Kyung Min Kim, Seung Ryul Lee, Man Chang, Eunju Cho, Young-Bae Kim, Chang Jung Kim, U. In Chung, and In-Kyeong Yoo. "Physical electro-thermal model of resistive switching in bi-layered resistance-change memory". *Scientific Reports*, 3:1680–1 – 1680–6, Apr 2013.

[18] Kim, Yunseok, Evgheni Strelcov, In Rok Hwang, Taekjib Choi, Bae Ho Park, Stephen Jesse, and Sergei V. Kalinin. "Correlative Multimodal Probing of Ionically-Mediated Electromechanical Phenomena in Simple Oxides". *Scientific Reports*, 3:2924–1 – 2924–7, Oct 2009.

[19] Kwon, Jung-Dae, Se-Hun Kwon, Tae-Hoon Jung, Kee-Seok Nam, Kwun-Bum Chung, Dong-Ho Kim, and Jin-Seong Park. "Controlled growth and properties of p-type cuprous oxide films by plasma-enhanced atomic layer deposition". *Applied Surface Science*, 285:373–379, Nov 2013.

[20] Lee, Yun Seog, Mark T. Winkler, Sin Cheng Siah, Riley Brandt, and Tonio Buonassisi. "Hall mobility of cuprous oxide thin films deposited by reactive direct-current magnetron sputtering". *Applied Physics Letters*, 98:192115–1 – 192115–3, 2011.

[21] Leng, Y. *Materials Characterization*, chapter 4. Wiley Publishing, Inc., Singapore, 2008.

[22] Li, Alex. "Tamper Induced Phase Transitions in Protective Materials for WMD-Related Sensing and Monitoring", 2012. Project Proposal to DTRA.

[23] Lv, Hangbing, Ming Wang, Haijun Wan, Yali Song, Wenjing Luo, Peng Zhou, Tingao Tang, Yinyin Lin, R. Huang, S. Song, J. G. Wu, H. M. Wu, and M. H. Chi. "Endurance enhancement of Cu-oxide based resistive switching memory with Al top electrode". *Applied Physics Letters*, 94:213502–1 – 213502–3, May 2009.

[24] Matsumura, Hideki, Asako Fujii, and Tomohiro Kitatani. “Properties of High-Mobility Cu2O Films Prepared by Thermal Oxidation of Cu at Low Temperatures”. *Japanese Journal of Applied Physics*, 35:5631–5636, Nov 1996.

[25] McDonald, N.R., S.M. Bishop, and N.C. Cady. “Experimentally Demonstrated Filament-based Switching Mechanism for Al/Cu x O/Cu Memristive Devices”. *Integrated Reliability Workshop Final Report (IRW), 2012 IEEE International*, 195–198. IEEE International, California, 2012.

[26] Meyer, B. K., A. Polity, D. Reppin, M. Becker, P. Hering, P. J. Klar, Th. Sander, C. Reindl, J. Benz, M. Eickhoff, C. Heiliger, M. Heinemann, J. Blsing, A. Krost, S. Shokovets, C. Mller, and C. Ronning. “Binary copper oxide semiconductors: From materials towards devices”. *Physica Status Solidi B*, 249:1487–1509, Jun 2012.

[27] Mohanty, S. “Memristors: From basics to deployment”. *IEEE Potentials*, 32, No. 3:765–783, May/June 2013.

[28] Morgan, D.V., M.J. Howes, R.D. Pollard, and D.G.P. Waters. “Electroforming and dielectric breakdown in thin aluminium oxide films”. *Thin Solid Films*, 15:123–131, 2012.

[29] Muñoz-Rojas, D., M. Jordan, C. Yeoh, A. T. Marin, A. Kursumovic, L. A. Dunlop, D. C. Iza, A. Chen, H. Wang, and J. L. MacManus Driscoll. “Growth of 5 $cm^2V^{-1}s^{-1}$ mobility, p-type Copper (I) oxide (Cu2O) films by fast atmospheric atomic layer deposition (AALD) at 225°C and below”. *AIP Advances*, 2:04179–1 – 04179–7, Dec 2012.

[30] Office of the Assistant Secretary of Defense for Nuclear Matters. “The Nuclear Matters Handbook”, 2011.

[31] Park, J.H. and K. Natesan. “Oxidation of Copper and Electronic Transport in Copper Oxides”. *Oxidation of Metals*, 39:411–435, Jan 1993.

[32] Pickett, Matthew D., Dmitri B. Strukov, Julien L. Borghetti, J. Joshua Yang, Gregory S. Snider, Duncan R. Stewart, and R. Stanley Williams. “Switching dynamics in titanium dioxide memristive devices”. *Journal of Applied Physics*, 106:074508–1 – 074508–6, Oct 2009.

[33] Sandia National Laboratories. “Report of the Weaponization and Weapons Production and Military Use Working Group”, 1997.

[34] Schindler, C., M. Weides, M.N. Kozicki, and R. Waser. “Low current resistive switching in CuSiO 2 cells”. *Applied Physics Letters*, 92:122910–1 – 122910–3, 2009.

[35] Strachan, John Paul, Dmitri B. Strukov, Julien Borghetti, J. Joshua Yang, Gilberto Medeiros-Ribeiro, and R. Stanley Williams. "The switching location of a bipolar memristor: chemical, thermal and structural mapping". *Nanotechnology*, 22, May 2011.

[36] Strukov, Dmitri B., Fabien Alibart, and R. Stanley Williams. "Thermophoresis/diffusion as a plausible mechanism for unipolar resistive switching in metaloxidemetal memristors". *Applied Physics A*, Mar 2012.

[37] Strukov, Dmitri B., Julien L. Borghetti, and R. Stanley Williams. "Coupled Ionic and Electronic Transport Model of Thin-Film Semiconductor Memristive Behavior". *Small*, 5, No. 9:1058–1063, 2009.

[38] Strukov, Dmitri B., Gregory S. Snider, Duncan R. Stewart, and R. Stanley Williams. "The missing memristor found". *Nature*, 453, May 2008.

[39] Timsit, Roland S. *Electrical Contacts: Principles and Applications*, chapter Chapter 1: Electrical Contact Resistance: Fundamental Principles. CRC Press, 1999.

[40] Toth, R.S. *Journal of Applied Physics*, 31, Issues 1112:1117, 1960.

[41] United Nations. "Treaty on the Nonproliferation of Nuclear Weapons", 1 July 1968.

[42] Walker, P. and W.H. Tarn. *Handbook of Metal Etchants*, chapter 2: Etchant Section. CRC Press, 1991.

[43] Wang, L. *Preparation and Characterization of Properties of Electrodeposited Copper Oxide Films*. Ph.D. thesis, University of Texas at Arlington, Arlington TX, 2006.

[44] Waser, Rainer, Regina Dittmann, Georgi Staikov, and Kristof Szot. "Redox-Based Resistive Switching Memories - Nanoionic Mechanisms, Prospects, and Challenges". *Advanced Materials*, 21:2632–2663, 2009.

[45] Wei, Mingzhen, Ning Lun, Xicheng Ma, and Shulin Wen. "A simple solvothermal reduction route to copper and cuprous oxide". *Materials Letters*, 61, Issues 1112:21472150, May 2007.

[46] Williams, R.S. "How we found the missing memristor". *IEEE Spectrum*, 29–35, Dec 2008.

[47] Williams, R.S. "Finding the missing memristor". Stanford University, YouTube, Nov 2011.

[48] Wong, H. S P, Heng-Yuan Lee, Shimeng Yu, Yu-Sheng Chen, Yi Wu, Pang-Shiu Chen, Byoungil Lee, F.T. Chen, and Ming-Jinn Tsai. "Metal-Oxide RRAM". *Proceedings of the IEEE*, 100:1951–1970, Jun 2012.

[49] Xu, Xin, Richard A. Register, and Stephen R. Forrest. "Mechanisms for current-induced conductivity changes in a conducting polymer". *Applied Physics Letters*, 89:142109–1 – 142109–3, Oct 2006.

[50] Yang, J. Joshua, Feng Miao, Matthew D. Pickett, Douglas A.A. Ohlberg, Duncan R. Stewart, Chun Ning Lau, and R. Stanley Williams. "The mechanism of electroforming of metal oxide memristive switches". *Nanotechnology*, 20, May 2009.

[51] Yang, J. Joshua, Matthew D. Pickett, Xuema Li, Douglas A. A. Ohlberg, Duncan R. Stewart, and R. Stanley Williams. "Memristive switching mechanism of metal/oxide/metal nanodevices". *Nature Nanotechnology*, 3:429–433, Jun 2008.

[52] Yang, J.J., Dmitri B. Strukov, and Duncan R. Stewart. "Memristive Devices for Computing". *Nature Nanotechnology*, 8, Jan 2013.

[53] Yang, W.-Y. and S.-W. Rhee. "Effect of electrode material on the resistance switching of Cu2O film". *Applied Physics Letters*, 91:232907–1 – 232907–3, Dec 2007.

[54] Yoon, Kyung Jean, Min Hwan Lee, Gun Hwan Kim, Seul Ji Song, Jun Yeong Seok, Sora Han, Jung Ho Yoon, Kyung Min Kim, and Cheol Seong Hwang. "Memristive tri-stable resistive switching at ruptured conducting filaments of a Pt/TiO2/Pt cell". *Nanotechnology*, 23, No. 18, 2012.

[55] Zens, Timothy. Instruction Slides on Atomic Force Microscopy for MATL 680, School of Engineering and Management, Air Force Institute of Technology, Wright Patterson AFB OH, 2013.

[56] Zhu, Hailing, Junying Zhang, Chunzhi Li, Feng Pan, Tianmin Wang, and Baibiao Huang. "Cu2O thin films deposited by reactive direct current magnetron sputtering". *Thin Solid Films*, 517:5700–5704, Mar 2009.

Vita

Second Lieutenant James P. Orta graduated as the salutatorian at Kubasaki High School on Camp Foster, Okinawa, Japan in 2007. He proceeded to the University of Washington with an AFROTC Scholarship and a skateboard where he studied long distance running, dinner-table debate etiquette, sailing, electric guitar, and the Seattle bus system, but only earned his Bachelor of Science in Electrical Engineering. Upon graduating and commissioning into the USAF, James was assigned to Wright-Patterson AFB to attend the Air Force Institute of Technology to study for a Master of Science in Electrical Engineering. Upon completion of his studies, he will travel to Colorado Springs where he will build skills in rock-climbing, muay thai, and skiing; and will work in Operational Test and Evaluation at Detachment 4, Peterson AFB.

REPORT DOCUMENTATION PAGE

Form Approved
OMB No. 0704-0188

PLEASE DO NOT RETURN YOUR FORM TO THE ABOVE ADDRESS.

1. REPORT DATE *(DD-MM-YYYY)*	2. REPORT TYPE	3. DATES COVERED *(From - To)*
27-03-2014	Master's Thesis	Oct 2012 - Mar 2014

4. TITLE AND SUBTITLE

Electrical Characterization of Spherical Copper Oxide Memristive Array Sensors

5a. CONTRACT NUMBER

5b. GRANT NUMBER

HDTRA 14111143

5c. PROGRAM ELEMENT NUMBER

6. AUTHOR(S)

Orta, James P., 2d Lt, USAF

5d. PROJECT NUMBER

5e. TASK NUMBER

5f. WORK UNIT NUMBER

7. PERFORMING ORGANIZATION NAME(S) AND ADDRESS(ES)

Air Force Institute of Technology
Graduate School of Engineering and Management (AFIT/EN)
2950 Hobson Way
Wright-Patterson AFB OH 45433-7765

8. PERFORMING ORGANIZATION REPORT NUMBER

AFIT-ENP-14-M-40

9. SPONSORING/MONITORING AGENCY NAME(S) AND ADDRESS(ES)

Defense Threat Reduction Agency
Calvin Shipbaugh
8725 John J. Kingman Rd #6201
Fort Belvoir, Virginia
Salvin.Shipbaugh@dtra.mil

10. SPONSOR/MONITOR'S ACRONYM(S)

DTRA

11. SPONSOR/MONITOR'S REPORT NUMBER(S)

12. DISTRIBUTION/AVAILABILITY STATEMENT

Distribution Statement A. Approved for Public Release; Distribution Unlimited

13. SUPPLEMENTARY NOTES

This material is declared a work of the U.S. Government and is not subject to copyright protection in the United States.

14. ABSTRACT

A new System Protection (SP) technology is explored by using electrical and mechanical interference-sensing devices that are implemented with granular memristive material. The granular materials consist of oxide-coated copper spheres with radii of about 700 μm that are placed in contact to produce thin oxide junctions which exhibit memristive behavior. Processes for etching, which compared acetic acid and nitric acid etches, and thermal oxidation at 100°C are performed and compared to produce copper spheres with a copper oxide layer over the sphere surface. Oxidized copper spheres are tested as sensor arrays by loading into a capillary tube in an aligned arrangement. The spheres are held in contact to characterize current-voltage behavior for various oxide thicknesses with typical ROFF values in the megaohm range. Electrical characterization of the oxidized copper spheres reveal directly proportional changes to current-voltage hyseteresis in μW under compressive forces. The thinnest oxide exhibited changes of 8.3 to 21.2 μW over 9 mN while the thickest had a response from 0.4 to 2.5 μW over 22.3 mN.

15. SUBJECT TERMS

ZnO, thin-films, device scaling, subtractive etch, plasma-assisted etch

16. SECURITY CLASSIFICATION OF:			17. LIMITATION OF ABSTRACT	18. NUMBER OF PAGES	19a. NAME OF RESPONSIBLE PERSON
a. REPORT	b. ABSTRACT	c. THIS PAGE			Major Timothy W.C. Zens, PhD AFIT/ENP
U	U	U	UU	104	19b. TELEPHONE NUMBER *(Include area code)* (937) 255-6565 x4695 timothy.zens@afit.edu

Reset

Standard Form 298 (Rev. 8/98)
Prescribed by ANSI Std. Z39.18